Title

The Picosecond Dynamics of Electron-Hole Pairs in Graded and Homogeneous CdS{sub x}Se{sub 1-x} Semiconductors

Author

Hane, J.K.

Publication Date

1995-05-01

LBL-37379
UC-400

Lawrence Berkeley Laboratory
UNIVERSITY OF CALIFORNIA

CHEMICAL SCIENCES DIVISION

The Picosecond Dynamics of Electron-Hole Pairs in Graded and Homogeneous CdS_xSe_{1-x} Semiconductors

J.K. Hane
(Ph.D. Thesis)

May 1995

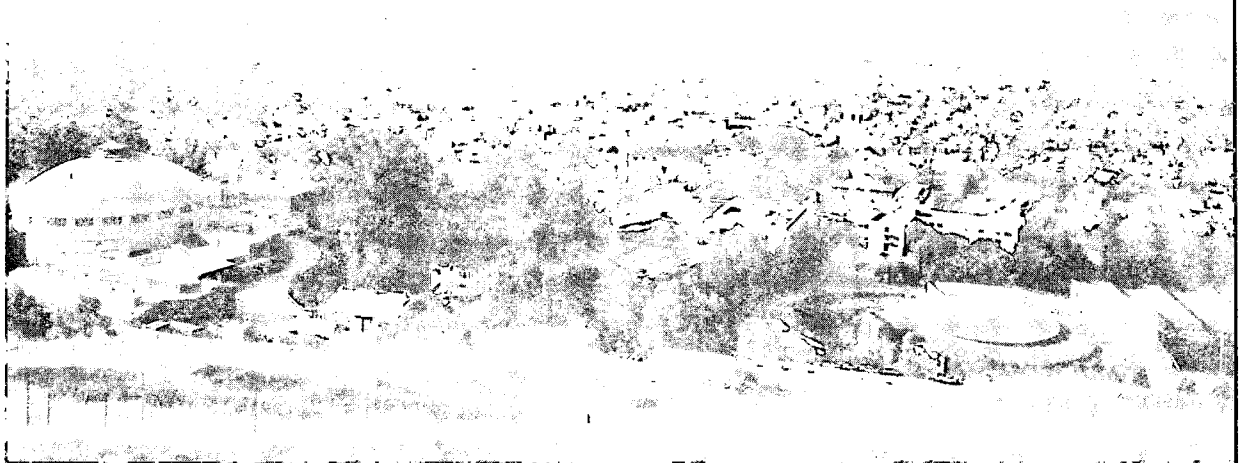

Prepared for the U.S. Department of Energy under Contract Number DE-AC03-76SF00098

DISCLAIMER

LBL-37379

The Picosecond Dynamics of Electron-Hole Pairs in Graded and Homogeneous CdS_xSe_{1-x} Semiconductors

by

Jennifer Kazuko Hane

Ph.D. Thesis

Department of Chemistry
University of California

and

Chemical Sciences Division
Lawrence Berkeley Laboratory
University of California
Berkeley, CA 94720

May 1995

This work was supported by the Laboratory Directed Research and Development Program of Lawrence Berkeley Laboratory under the U.S. Department of Energy, Contract No. DE-AC03-76SF00098.

The Picosecond Dynamics of Electron-Hole Pairs in

Graded and Homogeneous CdS_xSe_{1-x} Semiconductors

by

Jennifer Kazuko Hane

The Picosecond Dynamics of Electron-Hole Pairs in Graded and Homogeneous CdS_XSe_{1-X} Semiconductors

by

Jennifer Kazuko Hane

Abstract

This thesis investigates the picosecond dynamics of electron-hole pairs in CdS_XSe_{1-X} semiconductors. A thorough examination of the wavelength and composition dependence of the time resolved luminescence was performed. These studies probed the effects of a macroscopic composition gradient, as well as those of the microscopic alloy disorder, on the e^--h^+ pair dynamics. Inhomogeneous, or "graded", samples possess a composition which varies as a function of distance from the surface. Materials with both increasing and decreasing S content with distance from the surface were examined, where "x" varied over the full range, $0 \leq x \leq 1$. In these graded materials, the band gap energy also varies as a function of position. Hence, the luminescence emission at various wavelengths serves as a probe of the diffusion of photoexcited e^--h^+ pairs. The graded semiconductor luminescence shows strong wavelength dependence, demonstrating diffusion in both band gap and concentration gradients. Furthermore, the data reflect a dependence on the dynamics of the e^--h^+ pairs at various compositions within the gradient. Specifically, a bottleneck in the diffusion is attributed to localization occurring

primarily in the compositions with the greatest degree of alloy disorder, i.e. around $CdS_{.50}Se_{.50}$.

Homogeneous crystals, with fixed composition, were studied for x = 0, .25, .50, .75, and 1. The data demonstrate a strong dependence of the time resolved luminescence on the composition. The mixed composition materials possess longer decay constants relative to the binary composition materials, CdS and CdSe. The observed trend in lifetimes agrees with a picture of localized states induced by the alloy compositional disorder. Within the luminescence profile of a given homogeneous crystal, no wavelength dependence of the time decays was observed. The dependence of the luminescence on composition was investigated further via picosecond luminescence upconversion spectroscopy. The development of this technique and its applicability to problems in semiconductor dynamics are presented in detail. Alloy materials with compositions x= 0, .25, and .50 were probed with improved time resolution. A high degree of nonexponential character in the decay functions was observed in the alloy materials. This long time tail of the luminescence in the alloy compositions can be attributed to a broad distribution of relaxation times, as modeled by the Kohlrausch exponential.

TABLE OF CONTENTS

LIST OF FIGURES

ACKNOWLEDGEMENTS

I would like to acknowledge the many people who have contributed to the research presented in this thesis. I would especially like to thank my partner in the majority of this project, Steve Gadd, for our long collaboration and for his crucial contributions to this work. My partner in the early stages of this project was Professor Michael Prisant. The project was initiated as a collaboration with Professor A. B. Ellis and coworkers at the University of Wisconsin, namely Jerry Meyer and Larry Leung. The two group mates who taught me much about the lasers and equipment when I was starting out in the group were Walter Merry and Robert Jordan. I would like to thank everyone above for all of their invaluable contributions to this project. It would not have been possible without their help. I would also like to thank all of the members of the Harris group, with whom I overlapped, who made the group such an enjoyable working environment. I wish I had time to acknowledge you all here, but I hope you know how much I appreciate both the scientific interactions and your friendship. Vijaya Narasimhan has been invaluable in the day-to-day operations of the group as well as always offering her encouragement. Finally, I would like to thank my advisor Professor Charles B. Harris, for his guidance and support. My financial support was paid by a Lawrence Berkeley Laboratory LDRD grant, and also in part, by the National Science Foundation.

I would also like to thank my family for their support during my graduate career. My parents Mikiso and Rose, my sister Laurie, and also, all of my extended family here in California have been greatly supportive during this long process. Also, I would like to

thank two of my graduate school classmates in particular, Art Mahoney and John Gehlen, who have shared much of graduate school with me.

I. Introduction

This thesis investigates the relaxation dynamics of electron-hole pairs in a II-VI semiconductor system, the CdS_xSe_{1-x} materials. These materials exist over the entire composition range, $0 \leq x \leq 1$, and possess strong, visible photoluminescence. Thus the CdS_xSe_{1-x} material is a good model system for examining the dependence of optical and transport properties on composition. The technique utilized for these studies is energy and time resolved luminescence. These studies are of interest for several reasons. First, from a materials chemistry perspective, it is a challenge to determine how to "tune" the composition of a material for a particular property. A systematic study of the dependence of carrier relaxation as a function of composition provides information on this question. Furthermore, semiconductor materials are primarily of interest for their electronic and optical properties. Hence, the dynamics of electron-hole pairs subsequent to optical excitation are relevant in determining potential applications. The II-VI materials possess larger band gap energies than the corresponding III-V materials, and thus are often proposed for applications requiring visible wavelengths, such as display devices and laser diodes. Finally, studies on the relaxation of carriers in semiconductors increase our fundamental understanding of processes in condensed phase. In particular, ultrafast optical spectroscopies have elucidated the relaxation processes subsequent to a short, laser pulse excitation.

Charged carriers created in a semiconductor by a short laser pulse (e.g. 10^{-14} to 10^{-12}) undergo many relaxation processes. The earliest time scale events are "orientational" relaxation, such as phase and spin relaxation. Energy relaxation involves

both intra- and interband relaxation. Electrons and holes rapidly and efficiently relax to the minima of their respective bands. This relaxation is accommodated through phonon excitations. Finally the electron-hole pair population undergoes interband relaxation by a combination of nonradiative and radiative channels. All of these processes are amenable to study via optical spectroscopies, though investigations on the fastest events have only been feasible in the past decade. This thesis investigates diffusion and energy relaxation which occur on the picosecond time scale. This work required development of luminescence measurement techniques with picosecond time resolution. In particular, a picosecond luminescence upconversion spectrometer was constructed for these studies. This technique is discussed in detail in Section III.

Furthermore, the CdS_xSe_{1-x} system serves as a model for fundamental alloy properties. The CdS_xSe_{1-x} alloys are more complex than elemental or binary composition materials, as they possess compositional disorder. Yet these alloys are more ordered than amorphous materials, since the atoms occupy regular lattice sites. Hence, these substitutional alloys bridge the gap between a perfect lattice and a completely disordered solid. As a result, some properties of the CdS_xSe_{1-x} system are merely a function of the average composition. Other properties require a description which depends on the microscopic features of the material.

This work explores the distinction between these two pictures, i.e. average and microscopic. For example, the steady state luminescence spectra shifts smoothly as a function of "x" between the spectra of the two binary components, CdS and CdSe. Clearly, in this instance, the band gap of the alloy may be described as a property of the average composition. However, the alloy disorder introduces a tailing of states into the

band gap. These states may serve to confine carriers to a shorter length scale, and hence make the electron-hole pairs sensitive to the local environment. Whereas, if the carriers are extended over a macroscopic distance, then they should be influenced by the average. Both of these regimes are investigated in this thesis.

II. Background

A. Materials

The particular system investigated in this thesis is the CdS_xSe_{1-x} alloy semiconductors. These materials are convenient for experimental studies for several reasons. The materials are semiconducting over the entire composition range, $0 \leq x \leq 1$. They possess the same band structure, a hexagonal wurtzite. The lattice parameters vary from $a = 4.14$ and $c = 6.72$ Å for CdS to $a = 4.30$ to $c = 7.01$ Å for CdSe. The band gap is direct and increases monotonically from 1.7 eV for CdSe to 2.4 eV for CdS.[1-6] Due to the rapid intraband relaxation of photoexcited carriers, the region of interest in these materials is centered around the valence band maximum and the conduction band minimum. That is, the states around the direct gap transition play the most important roles. In this region, the band dispersion is approximately parabolic. The conduction band states are generated from the s-like states of the cadmium, and the valence band states originate from the p-like states of the sulphur and selenium. The crystal field and spin-orbit interactions split the valence band into three sub-bands, the heavy-hole, light-hole, and split-off sub-bands. See Figure 1 for a schematic diagram of the states of interest in these experiments.

The band structure of alloy semiconductors has been calculated with various methods.[7-9] The main feature of interest is the variation of the band gap energy with composition. The virtual crystal approximation is a first order perturbation picture, which treats the crystal potential as a weighted average of all possible configurations of

Figure 1. Schematic band diagram for the region around k=0 in the CdS_xSe_{1-x} semiconductors. The valence band is split into the three sub-band: the heavy hole (hh), light hole (lh), and split-off (so) sub-bands. The arrows indicate the experimental configuration. Ultraband gap energy photons excite electrons from the valence bands into the conduction band. The hot electron and hole populations undergo rapid intraband relaxation. Finally the electrons and holes radiatively recombine from states near the minima of their respective bands. This emission, at an energy characteristic of the band gap, is the measured luminescence.

SCHEMATIC BAND DIAGRAM

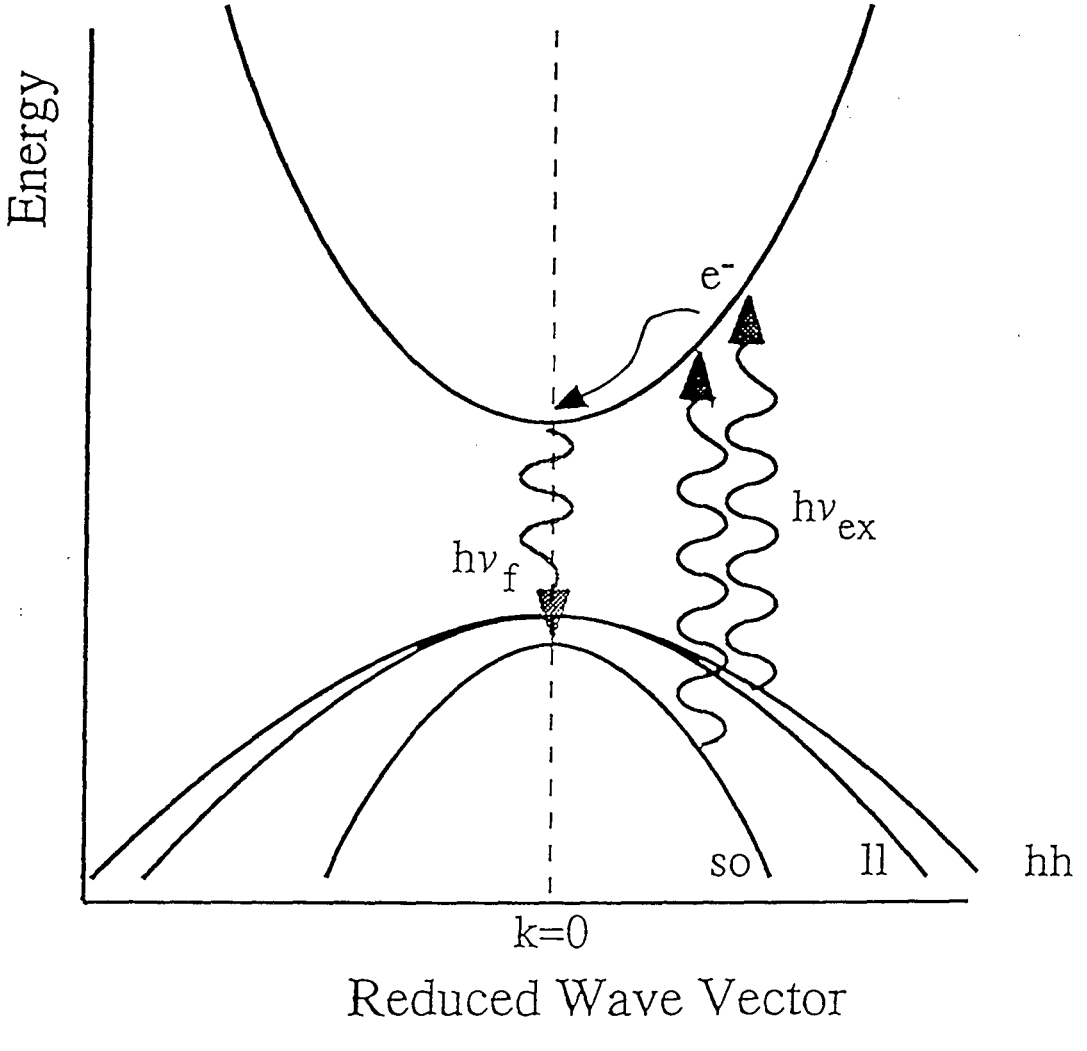

atoms at the lattice sites.[10-13] This average picture has been found adequate to describe the variation of band gap energy, or "bowing" that is seen in alloy materials.[14] This picture does not include localized states which are generated by disorder effects in compositional alloys. However, some tailing of the density of states into the gap has been accounted for with the virtual crystal method. These localized states are investigated in this thesis, and are discussed in Section V.

The CdS_xSe_{1-x} semiconductors fluoresce in the visible portion of the spectrum, from $\lambda_{max} \sim 718$ nm for CdSe to $\lambda_{max} \sim 508$ nm for CdS. The luminescence shifts smooth as a function of composition according to[15]:

$$\lambda_{max}\ (nm) = 718 - 210\,x \qquad (1)$$

The steady state spectra of these samples demonstrate this linear shift in luminescence maxima. Figure 2 shows the luminescence spectra of five compositions spanning the range $0 \leq x \leq 1$. The spectra are inhomogeneously broadened and possess a fwhm of ~ 30 nm. Due to their strong, visible luminescence, this system is conveniently probed by time resolved luminescence spectroscopy. Estimates of the quantum efficiency for these materials vary, the range is typically .05 to .0005 at room temperature.[16] Therefore, the main decay channel is nonradiative. In particular, we observe dependence on surface properties such as the finish. Other studies have probed the effects of surface adsorbates on luminescence in CdS and CdSe materials.[17-23] Hence, the surface states appear to be an important nonradiative decay channel.

Two types of materials were examined in this work. Inhomogeneous, or "graded" composition samples, are materials whose composition is position dependent. In thiscase, the composition varies as a function of distance from the surface. We assign

Figure 2. The steady state luminescence spectra of five homogeneous CdS_xSe_{1-x} semiconductors with compositions x= 0, .25, .50, .75, and 1. The spectra are inhomogeneously broadened, with the peak emission occurring at approximately the wavelength given in Equation 1.

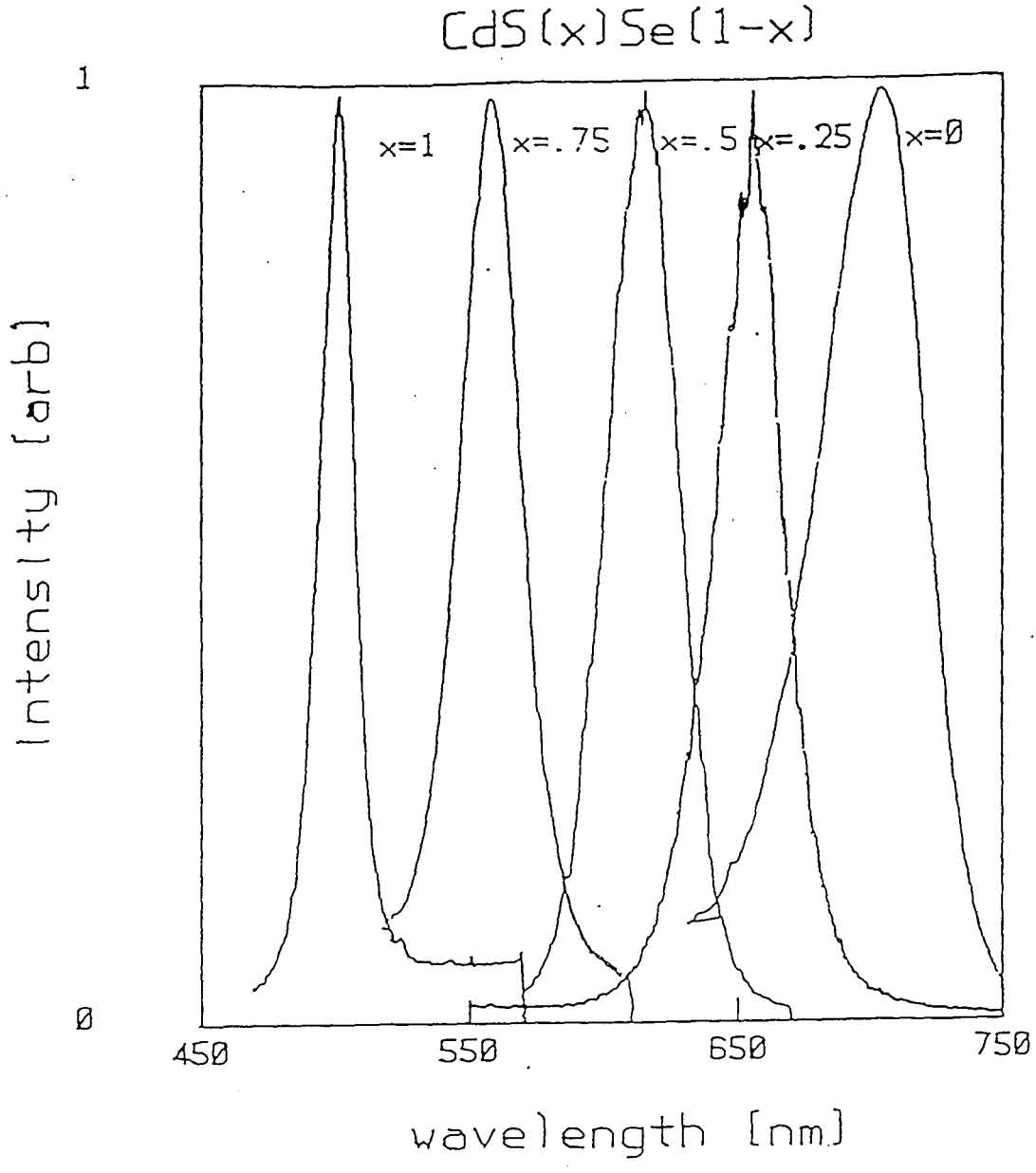
CdS(x)Se(1-x)
1
0
x=1
x=.75
x=.5
x=.25
x=0
Intenslty [arb]
450
550
650
750
wavelength [nm]

different names to two types of gradients for clarity. We distinguish between "CdSe/S" and "CdS/Se" materials in this work. CdSe/S describes a material with CdSe as a substrate. The surface is S-rich, and decreases in concentration until the pure CdSe substrate is reached. Thus the band gap decreases as a function of distance from the surface. The oppositely graded material, CdS/Se, possesses an increasing potential gradient with distance from the surface. The surface is Se-rich and the substrate is CdS. Homogeneous materials are samples with a particular value of "x", and hence possess an average composition throughout. Five distinct compositions were examined in this work, x = 0, .25, .50, .75, and 1.

Graded samples were obtained from Ellis and coworkers from the Chemistry Department at the University of Wisconsin at Madison. The materials were synthesized with a solid state, vapor phase diffusion method.[24-27] Briefly, the CdSe/S samples were grown from a single crystal, n-type CdSe substrate obtained from Cleveland Crystals. The substrate was initially chemically etched to expose a fresh surface. The CdSe was sealed in an evacuated tube with S and heated to 700 °C for 15 minutes to 1 hour. Different heating times produce composition gradients of varying thickness. The CdSe/S was then post-treated by heating in the presence of Cd, again at 700 °C for 15 minutes. It was observed that materials heated only in the presence of S were not electrically conductive. Presumably, a high concentration of Cd vacancies, which act as acceptors, are present if the material is not treated with Cd. Similarly, the CdS/Se materials were synthesized from CdS substrates by heating with Se and then Cd.

The graded CdS_xSe_{1-x} samples have ~ 1-μm thick graded regions. For CdSe/S specimens, the graded zone comprises virtually all of the alloy compositions from x = 1

at the surface to x = 0 in the substrate; for CdS/Se, the compositions vary from x~ 0.2 at the surface to x = 1 in the substrate. The thickness of the gradients were characterized by Ellis and coworkers. The sample was degraded by Argon ion sputter etching at a fixed rate. The rate was determined from measured step heights on a CdS control sample. The composition was monitored during the sputtering with Auger electron spectroscopy. The luminescence spectra of the graded material were also used to qualitatively confirm the composition profile. The materials were chemically etched with Br/MeOH solution in a several step process. With each subsequent etch, the spectrum shifted toward the substrate luminescence. Further details of the synthesis and characterization can be found in the literature.[28-30]

The homogeneous crystals were obtained commercially from Cleveland Crystals, who produce them with a bulk vapor phase diffusion technique. All samples were n-type, low resistivity crystals having hexagonal structure with the c-axis perpendicular to the surface plane. In the experiments on homogeneous materials, it was observed that the surface finish affected the luminescence times. This effect is probably due to the role of surface states as nonradiative decay channels. The upconversion experiments were performed on materials which were cleaved by us in order to produce a surface of good optical quality, but not mechanically polished. The crystals possess two cleavage planes. Pieces were typically cleaved perpendicular to the c-axis (i.e. an a-face) with the edge of a razor blade.

B. Proposed Experiments

The aim of this thesis is to examine the dynamics of photoexcited carriers in these CdS_xSe_{1-x} semiconductors. An ultraband gap energy, picosecond laser pulse creates a nonequilibrium distribution of electrons and holes. (Also, see Figure 1.) The relaxation processes this population undergoes can generally be broken into three phases. The separation is not distinct. These processes all occur simultaneously, but are characterized by different time scales. In these experiments, typically an ultraviolet excitation source, with photon energy of ~ 4 eV, is used to populate the conduction band. This energy is far above the band gap of 1.7-2.4 eV. Hence the population is generated with excess kinetic energy, i.e. high up in the conduction band. Due to momentum and energy selection rules, the initial population is centered around a narrow distribution in energy and in k-space. That is, the optical transition conserves momentum for $\Delta k=0$. The first relaxation process this population undergoes involves the loss of this phase coherence with the driving field. Any scattering event, elastic or inelastic, serves to randomize the phase. This process generally occurs in a few picoseconds or in the subpicosecond regime, depending on experimental conditions. In this step, the distribution achieves a quasi-equilibrium, but the population is still "hot" compared to the lattice temperature. Hence, the second part of the relaxation process involves intraband energy relaxation, predominantly loss of energy to the phonon modes of the lattice. This process also occurs on the subpicosecond to tens of picosecond time scale. Finally, the nonequilibrium population undergoes interband relaxation, or returns to the valence band.

Several interband relaxation mechanisms exist, involving both radiative and nonradiative decay channels. This step occurs in the picosecond and nanosecond regime. Nonradiative paths involve a continuum of states, such as a high density of surface states or defect states. Radiative relaxation involves electron and hole recombination from near band edge states. This luminescence is the detected signal for the experiments described in this thesis. Of course, the time dependence of the luminescence reflects the dynamics of all relaxation processes. Hence, the signal may be complex if several mechanisms occur on competitive time scales. The techniques used to time resolve the signal include time-correlated single photon counting and luminescence upconversion.

The luminescence experiments in the this work provide information on the relaxation processes in CdS_xSe_{1-x} in particular, and II-VI semiconductors in general. In the graded composition samples, the behavior of carriers in an internal potential gradient is probed. Electron-hole pairs are generated in the near surface region of the sample. Diffusion in both concentration and band gap gradients occurs. The emission at a particular depth, and hence composition, serves as a color coded indicator of the spatial origin of the luminescence. In this manner, the evolution of the distribution of carriers is monitored. By examining both CdSe/S and CdS/Se graded samples, diffusion driven by and opposed to a potential gradient are probed.

Experiments on the homogeneous materials provide more details on the dynamics which occur at a given composition. Luminescence from the near band edge states serve as a probe of the local environment. In an alloy, the compositional substitution generates local potential fluctuations. Hence, disorder induced localized states are present in alloy materials. The density and depth of these states will depend on the amount of disorder

present. This thesis examines five distinct compositions in the CdS_xSe_{1-x} series with varying degrees of alloy substitution. The effects of localized states on the relaxation dynamics of electron-hole pairs in these materials are studied. Together, these two sets of studies, on inhomogeneous and homogeneous materials, provide a complementary picture of the transport and relaxation dynamics in the CdS_xSe_{1-x} semiconductor system. Diffusion through a macroscopic potential gradient is probed, as well as the effect of microscopic potential fluctuations arising from compositional disorder at each particular composition in that gradient.

The technique chosen for these studies, time resolved luminescence, is not the only ultrafast optical spectroscopy which is appropriate for investigating carrier dynamics. Often, the choice of technique is influenced by purely experimental considerations, such as equipment, wavelengths available from lasers, and signal detection. Time resolved luminescence has been widely applied to these materials, as well as other direct band gap semiconductors, due to their bright, visible fluorescence. Luminescence spectroscopy is an excellent probe of the energy distribution of carriers in the system. Another technique which has been applied to the relaxation of photoexcited carriers is the pump probe type experiment.[31-36] In this case, the transient absorption of electrons pumped into the conduction band is monitored with the probe laser pulse. This type of experiment yields similar information on the cooling of the hot electron population and subsequent interband relaxation. Additionally, certain four-wave mixing techniques have also been applied to the CdS_xSe_{1-x} system, to monitor both phase relaxation and carrier diffusion.[37-49]

III. Time Resolved Luminescence Techniques

A. Details of Picosecond Laser System

The experiments were performed with the following picosecond laser system. A mode-locked Coherent Antares 76-Series Nd:YLF served as a pump laser for a two-jet dye laser. The fundamental frequency of the YLF is doubled to serve as the pump laser at 527 nm. The output is typically 70 ps and possesses an average power between 2.0 and 3.0 W. In order to produce output power above 2.0 W, a Coherent SHGTC heated doubling crystal unit was added to the laser system. The 527 nm light is used to synchronously pump a Coherent 700 Series dye laser. This laser was operated both in single and two jet modes. The output was cavity dumped at a repetition rate of 3.8 MHz with a Coherent 7200 Cavity Dumper. Typical output for single jet operation was 6 to 10 ps, with an average power of 250 to 300 mw. For dual jet use, the best results are obtained with the dye laser combination of R6G and DODCI. Narrow pulse widths could be obtained, but with a sacrifice in average power. Typical results were 1 ps pulses with average power of 150 to 200 mw (~ 40-50 nJ per pulse).

Achieving short pulses with high power requires simultaneously balancing the saturable absorber concentration and the pump power. A fair amount of testing was performed to optimize for both time resolution and power. At the powers operated, saturable absorber dye was fairly rapidly photo-decomposed. Pulses were noticeably broadened during the course of an experiment of six hours, for example. Small amounts

of concentrated dye were added to optimize pulse shape when critical. A commercial autocorrelator, Femtochrome, was used to monitor the pulse.

The most frequently used dye is Rhodamine-6-G, as it possesses the highest gain coefficient and is the most stable. To access a broader range of wavelengths, a few other dyes were used in this work. DCM was used for wavelengths further to the red. In particular, it was utilized at 630 nm, the maximum gain. (R6G's maximum gain is at 590 nm.) For a few experiments, where the visible output of the dye laser was used to directly excite the lower band gap semiconductors, laser output further to the blue was desired. Rhodamine 560 was used in a few experiments included in this work. This dye is considerably less stable than R6G, and was often seen to degrade over the course of 2-3 days. This degradation causes a precipitous drop in output power. The degradation is evidenced by the dye solution turning from clear yellow to an opaque orange-brown. It has been suggested that R560 reacts with brass fittings in dye reservoirs, and the reduction or elimination of brass parts may extend the useful lifetime of the dye solutions.

B. Time-Correlated Single Photon Counting

The technique of time-correlated single photon counting (TCSPC) is well established for measuring fast luminescence lifetimes.[50-57] Though TCSPC is a common technique, this work required optimizing the equipment for the fastest time response. Hence, this section will include some practical information for setting up and utilizing this method. Furthermore, some comparison of luminescence methods will be

useful to distinguish this technique from upconversion, which is also discussed in this thesis.

This technique utilizes timing electronics to measure the luminescence lifetimes in the following way. A high-repetition rate laser, consequently operating at relatively low power, is used to initiate an excited state population. The fluorescence from the sample is collected and subsequently detected by a fast photomultiplier tube. The output of this detector is used to trigger the initiation of a voltage ramp. This ramp is terminated by the arrival of a stop pulse. The stop pulse is the output of a photodiode which has been triggered by the same laser pulse train used to excite the sample. Hence the height of the voltage ramp is related to the time between absorption of the excite and emission of the luminescence photon. Single events are detected thousands of times, the voltage ramps are sorted by size with a multichannel buffer, and a histogram of the probability of emission with time is generated. This data represents the luminescence decay time of the sample.

One of the keys to this technique is to utilize a high-repetition rate, low peak power laser, such that the number of events detected per laser shot is either one or zero. This requirement is due to photon counting statistics. Under conditions where more than one event per laser shot is generated, only the earliest photon will trigger the voltage ramp. Hence, the histogram generated will reflect a bias toward early time events. Thus, in single photon counting, the experiments are performed at signal levels that are no more than one event per one hundred laser shots.

The configuration of our system for time-correlated single photon counting is as follows. See Figure 3 for a schematic of the experiment and Figure 4 for a block diagram

Figure 3. Time-correlated single photon counting system. A mode-locked, YLF laser operating at 76 MHz is frequency doubled and used to pump a cavity dumped dye laser. Typical output consists of ~ 5 ps pulses at 630 nm, cavity dumped at 3.8 MHz. A small portion of this laser beam is split off at the beamsplitter (BS), passed to a photodiode (PD), and utilized to establish the timing coincidence. The main portion of the beam is frequency doubled. The ultraviolet light at 315 nm is focused onto the semiconductor sample (XTAL) at an oblique angle. The fluorescence is collected, passed through a monochromator (MC), and detected in single photon counting mode with a microchannel plate photomultiplier tube (MCP). The data collection is controlled by computer (PC).

TIME-CORRELATED SINGLE PHOTON COUNTING

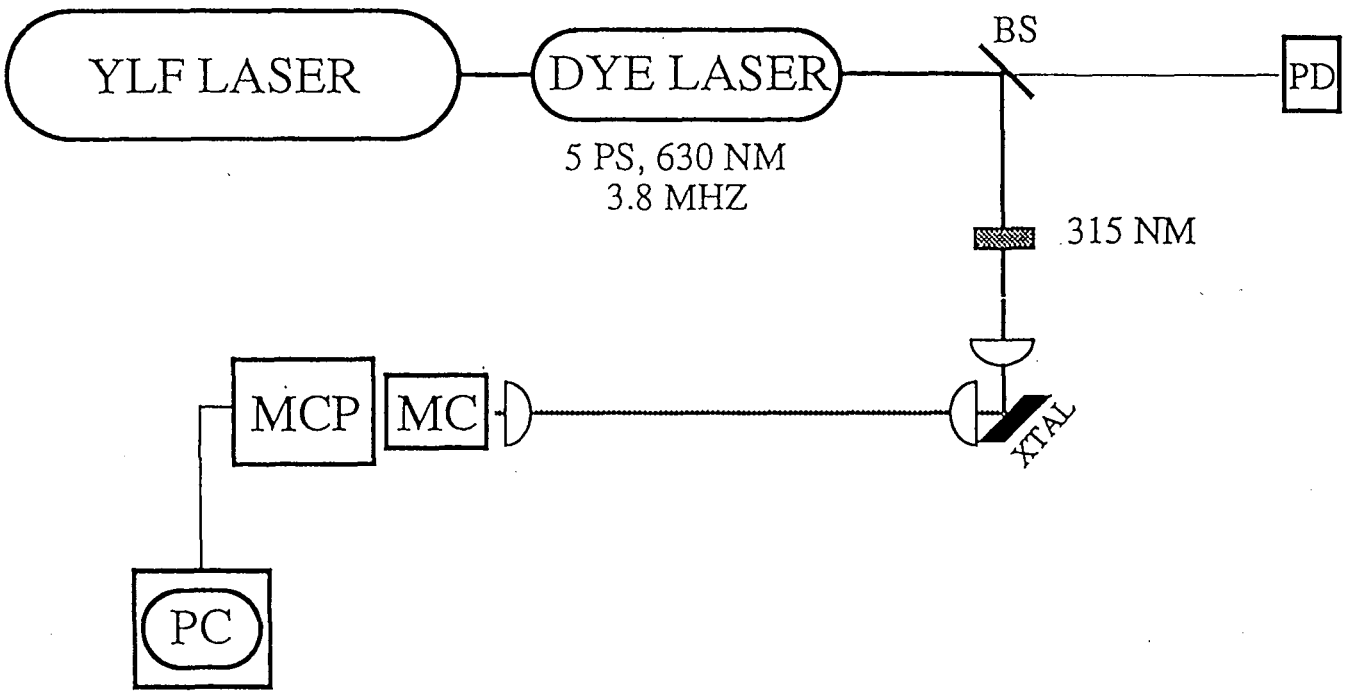

Figure 4. Block diagram of the electronics for time-correlated single photon counting detection. The semiconductor luminescence is detected with a microchannel plate photomultiplier tube (MCP), passed to a Hewlett-Packard GHz pre-amplifier (AMP), followed by a constant fraction discriminator (DISC). This output is used to trigger the start of a voltage ramp in the time-to-amplitude converter (TAC). The stop pulse originates from the laser pulse train, which is used to trigger a photodiode (PD) whose output is sent to the TAC. The output of the TAC is sorted by the multi-channel buffer (MCA). The data collection is controlled by computer (PC).

BLOCK DIAGRAM OF TCSPC DETECTION

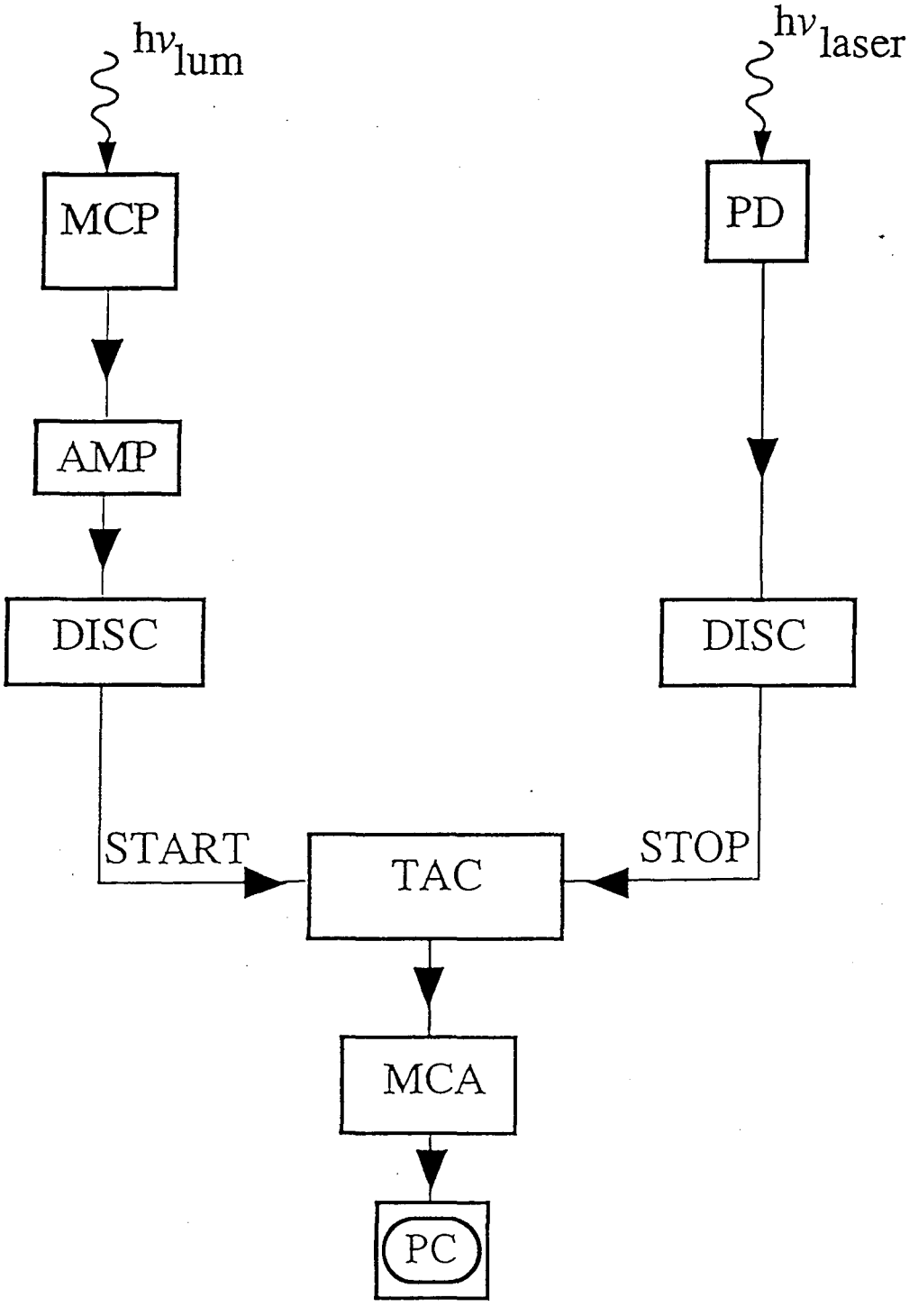

of the electronic detection. The visible output of the dye laser system described above was frequency doubled with a $LiIO_3$ crystal to produce 315 nm excite pulses. The fundamental was filtered and the remaining uv pulse was focused at an oblique angle onto the semiconductor face. A bright fluorescent spot was visible by eye on the crystal surface. A KV-470 filter was used to block scattered uv in front of a low f-number aspheric lens. The light was recollimated and focused onto the slit of a .10 m ISA single pass monochromator, which was mounted on the front of the phototube housing. A Hamamatsu microchannel plate, R1564U, was used for fast, single photon detection. The signal was passed through a two stage GHz pre-amplifier, a 8447D Hewlett-Packard model. This output was sent to an Ortec Model 583 constant fraction discriminator. The timing coincidence was established by monitoring the visible laser pulse with a fast EG&G FND-100 photodiode connected to a second Ortec discriminator. The time-correlated single photon counting signal was collected by using the two Ortec outputs to trigger a Canberra 2043 time-to-amplitude converter which was interfaced to an ADAC Model 1023 analog-to-digital converter functioning as a multichannel analyzer. The data collection was controlled by a computer.

The instrument response function of this system was determined by scattering visible laser light from the surface of the sample. The instrument function determines the fastest possible time-resolution which can be obtained with the particular experimental set-up. Generally, if the measured decay times are approximately ten times longer than the instrument function, it is usually neglected in the fitting of the data. However, if the instrument function is on a similar time scale as the data, then one must consider the effects of the instrument function. In some cases, we were measuring samples with

characteristic time constants less than 100 ps. Hence, we were interested in obtaining the highest possible time resolution available with this technique.

The features which were most important to obtaining a fast instrument function are described below. The electronic response of the photon detector is important. The shape of the output pulse will determine, to a large extent, the instrument function. A microchannel plate is optimized for fast response, compared to a photomultiplier tube. The model we used produced output pulses with a .2 ns rise time, compared to at least a few ns for a typical photomultiplier tube. To avoid further broadening of the MCP output, the preamplifer should have GHz response. We had consistently reliable pulse shapes with the Hewlett-Packard amplifier. However, it proved to be a fairly sensitive piece of equipment, which could be damaged easily.

Constant fraction discrimination serves to improve the instrument function by triggering the voltage ramp over a narrower distribution in time. A constant fraction discriminator splits the incoming pulse into two segments. One is inverted and delayed, and then the two are readded together. The discriminator then sends an output pulse at the first zero crossing point (in voltage). If the shape of the incoming pulses are relatively constant (regardless of fluctuations in height), then this trigger point is defined more narrowly in time than the leading edge of the incoming pulse. By utilizing constant fraction discrimination, the leading edge of the instrument function decreases from a 1 ns rise time to 100 ps, a significant improvement.

The discriminator must be optimized for the threshold level and the delay between the divided pulses. A reasonable threshold level can be set without too much difficulty with the aid of a good oscilloscope. The timing delay has to be optimized with trial and

error. When using the relatively narrow pulses of the microchannel plate, the amount of externally added delay required (via BNC cable) is small.

Once the detector, fast amplifier, and discriminators have been optimized, the largest remaining problem for fast timing was triggering on satellite features of the microchannel plate pulse. The unamplified pulse directly out of the channel plate had ringing after the main feature. The effects of this ringing varied widely with threshold and delay settings of the discriminator. It was possible to see triggering primarily on the first ring instead of the main pulse. The setting could minimize triggering on the rings, but could not eliminate it altogether. Hence even the best instrument functions showed structure.

The structure in the instrument function added difficulty to the modeling and fitting of data. Figure 5 demonstrates the convolution of the instrument response with the decay function of the sample. The instrument function, in this case, possesses a 100 ps rise time and a full-width half max of ~ 70 ps. These values are fairly typical for TCSPC systems which have been optimized for picosecond luminescence. The time resolution stated for such systems may be significantly less than 70 ps, such as 20 ps.[58] Certainly a 20 ps luminescence lifetime convoluted with the instrument function will be distinguishable from the instrument function alone. Hence, the time resolution of the system will provide an upper bound for ultrafast decay times which are competitive with the instrument function. However, on time scales comparable to the instrument function, deconvolution and fitting of the data are difficult.

Basically, a numerical deconvolution of the instrument function and data proved unsuccessful due to the amount of structure in the instrument function. Although a fitting

Figure 5. Effect of the instrument function (lowest dashed line) on the TCSPC data collected for CdSe (other lines represent CdSe decays at several wavelengths). In this experiment, the luminescence signal is on the order of the instrument function. The CdSe decay functions reflect the convolution with the electronic ringing in the instrument function.

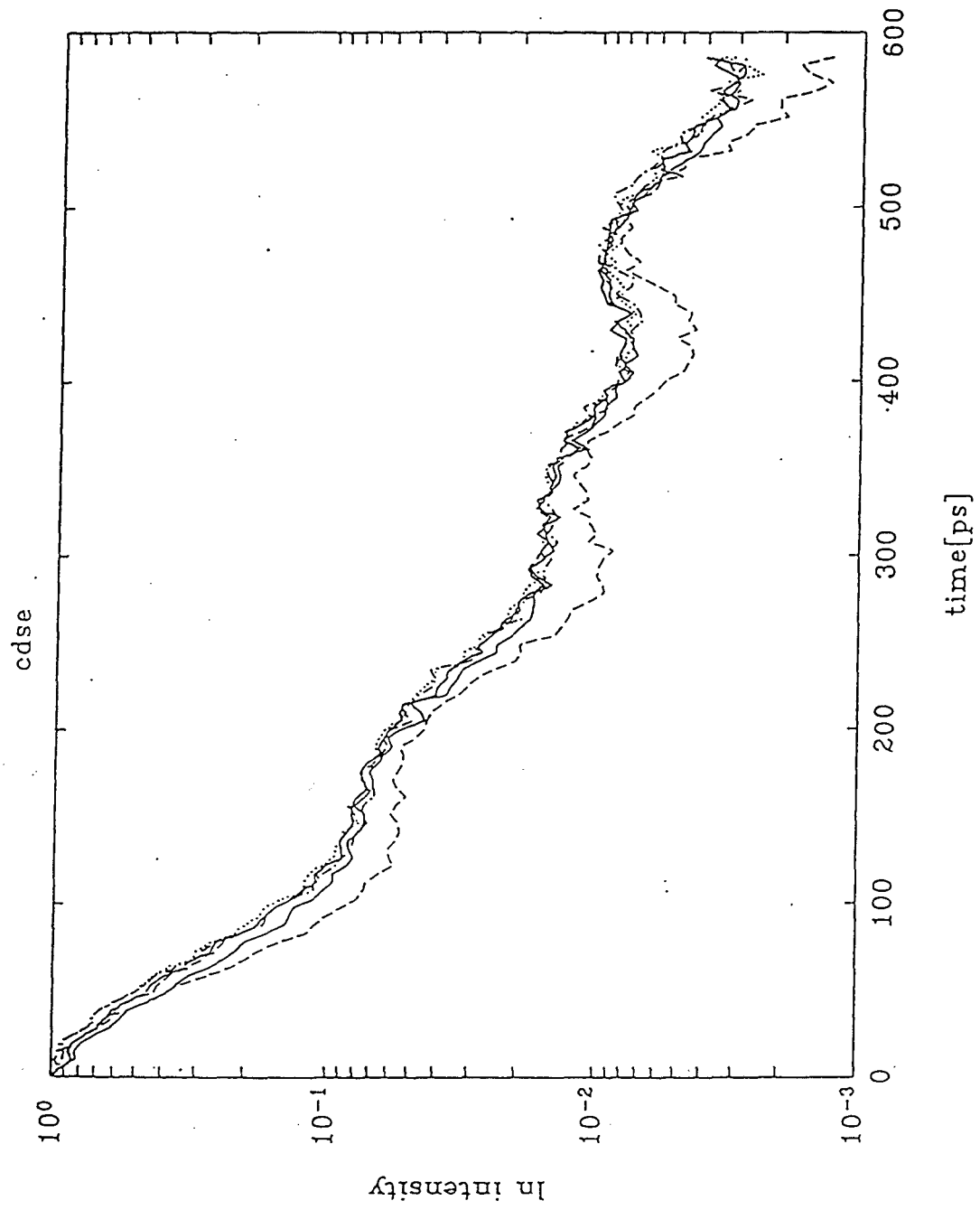
cdse
ln intensity
10^0
10^{-1}
10^{-2}
10^{-3}
0
100
200
300
400
500
600
time[ps]

program which includes deconvolution has been successfully implemented in this research group[59], it involves instrument functions which are assumed smooth and analytic, such as a Guassian or Lorentzian pulse shape. With the amount of features in the TCSPC instrument function, modeling must be done with an iterative forward convolution (of the instrument function with the model function) and subsequent fit.

This research was conducted at the limits of the time resolution provided by TCSPC, and much consideration was given to its application to ultrafast problems. The best features of TCSPC are its extremely high sensitivity and excellent signal-to-noise. Since signal counts are synchronized to the laser shot within a 20 ns window, dark counts are relatively low in this technique, < 5 counts per second. In semiconductor studies, one cannot utilize high power laser pulses to excite luminescence due to excessive heat deposition leading to damage. Hence, high repetition rate, low power laser systems are utilized, and such systems lend themselves well to single photon counting detection.

The limits of this technique are derived from its method of timing, the electronic detection. Ultimately, the time resolution is limited by features of the photon detector, the voltage pulse from the microchannel plate. No matter how much one optimizes the set-up for single photon counting, a few tens of picoseconds will be the lower limit to time resolution. Ultrafast spectroscopies which rely on path length variations in the laser pulse train are limited by the width of the laser pulse. Three orders of magnitude improvement in time resolution over TCSPC is possible with these techniques, which will be discussed in the subsequent section.

C. Luminescence Upconversion

1. General Discussion

Luminescence upconversion, also known as frequency upconversion or sum frequency generation, is a spectroscopic technique for time resolving fluorescence signals. Its development stems from the desire to obtain the fastest possible time resolution, which is comparable to the laser pulse width used to initiate the luminescence. The basis of this technique is to utilize the laser pulse train as an optical sampling gate. Fluorescence from the sample is collected and mixed with the laser pulse train in a nonlinear crystal, such as BBO (beta-barium borate) or $LiIO_3$ (lithium iodate). Under the appropriate energy and momentum matching conditions, the sum and difference frequencies of the two incoming sources may be generated. The theory of such nonlinear optical processes is discussed in several excellent references.[60,61]

In these experiments, we detect the upconverted signal, or the sum frequency. This process is represented in Figure 6. The luminescence and probe pulse must overlap in time and space inside the nonlinear crystal for the upconverted signal to be generated. A variable path length is introduced into one of the input signals, and in this manner, the laser pulse serves as an optical gate. The upconverted signal depends on the intensity of both the luminescence and the probe beam. If the laser source is stable, the upconverted intensity directly maps out the sample luminescence decay.

The time resolution of this technique is generated by varying the path length of a probe laser with respect to the sample fluorescence. All time-domain, laser spectroscopies with pulse-width limited resolution are based on such an optical delay.

Figure 6. Schematic diagram of the luminescence upconversion technique. The sum frequency is generated from the overlap of the semiconductor luminescence with the picosecond laser pulse, which acts as an "optical gate". This gating pulse is passed through a variable path length and overlaps with the luminescence at corresponding time delays, T_1, T_2, and T_3. The upconverted signal is proportional to both the luminescence and laser pulse intensity. If the laser pulse remains constant, the upconverted counts directly map back onto the original sample luminescence.

Luminescence Upconversion

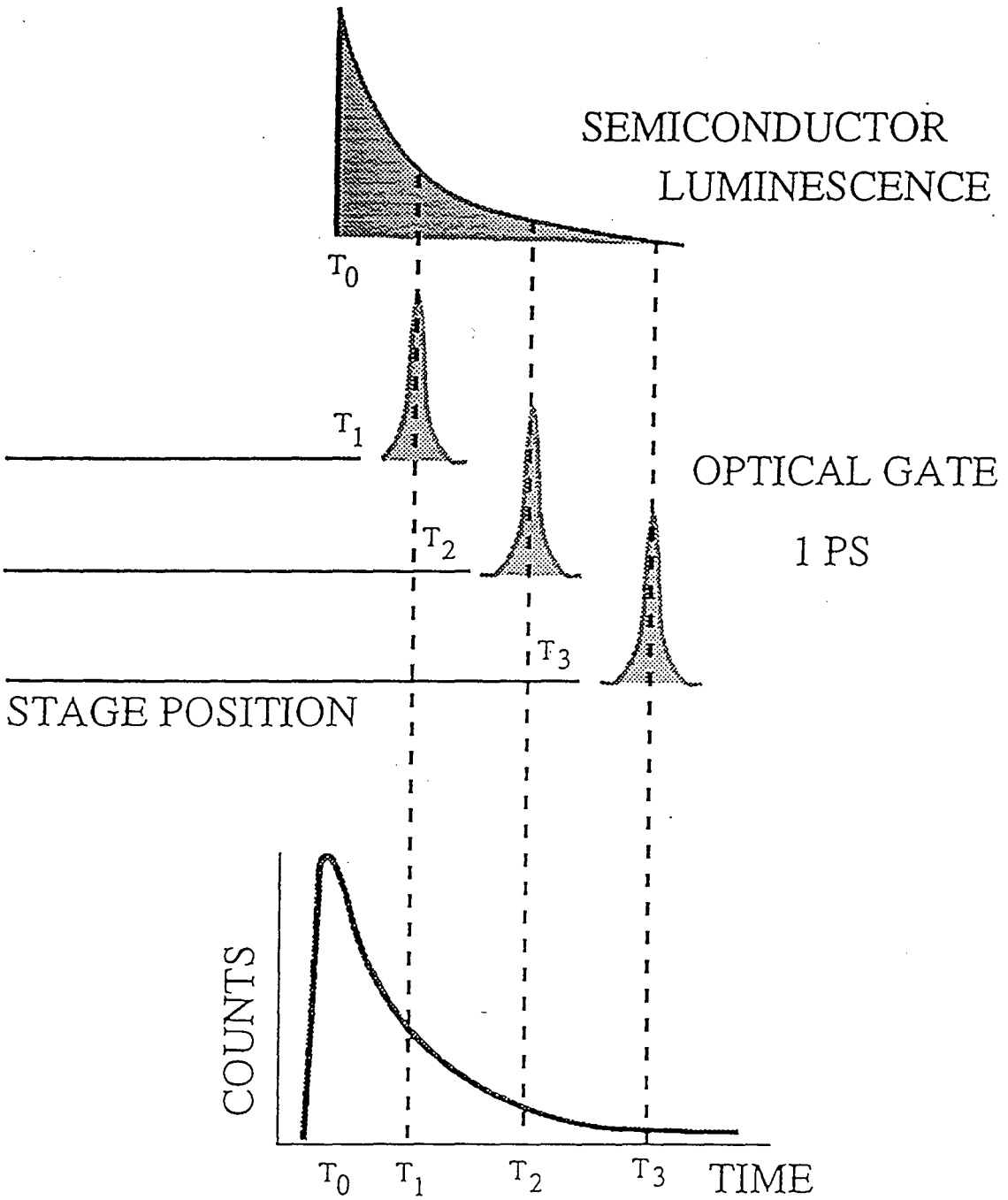

Introducing a variable path length is trivial, for example, 1 ps corresponds to a .3 mm distance. Controlling even micron distances with commercially available translation stages is routine. Hence, achieving the picosecond resolution is not difficult. The difficulty lies in generating the upconverted signal itself.

As a nonlinear optical process, frequency upconversion requires energy and momentum matching conditions:

$$\nu_f + \nu_p = \nu_s \tag{2}$$

$$\vec{k}_f + \vec{k}_p = \vec{k}_s \tag{3}$$

where ν_f, ν_p, and ν_s are the fluorescence, pump and sum frequencies of the light, and $\vec{k}_f$, $\vec{k}_p$, and $\vec{k}_s$ are the fluorescence, pump, and sum wave vectors of the light. In this thesis, we consider the case of collinear overlap of the fluorescence and pump beams. Following the development of Shah[62], for collinear geometry, the phase matching can be written as:

$$\frac{n_f}{\lambda_f} + \frac{n_p}{\lambda_p} = \frac{n_s}{\lambda_s} \tag{4}$$

where n_i is the refractive index at the wavelength λ_i. In anisotropic media, the index of refraction varies with direction of propagation. The nonlinear crystal utilized in the following experiments, BBO, is a uniaxial crystal. For the optical axis in the z-direction, $n_Z=n_e$ is termed the extraordinary index, and $n_X=n_y$ is the ordinary index. BBO is a

negative uniaxial crystal, meaning $n_e < n_o$. In general, at least one wave must propagate as an extraordinary ray in the nonlinear crystal in order to achieve phase matching. In the particular case of negative uniaxial materials, the sum frequency ray must be extraordinary. The upconversion experiments were performed with Type I phase-matching, for which the fluorescence and probe beams propagate as ordinary waves and the sum frequency ray is extraordinary. For this particular case (O + O $\rightarrow$ E), the phase matching angle, θ_m, is given by:

$$\sin^2\theta_m = \frac{\frac{1}{n_s^2(\theta_m)} - \frac{1}{n_{o,s}^2}}{\frac{1}{n_{e,s}^2} - \frac{1}{n_{o,s}^2}} \qquad (5)$$

where $n_s(\theta_m)$ is given by:

$$n_s(\theta_m) = n_{o,f}\frac{\lambda_s}{\lambda_f} + n_{o,p}\frac{\lambda_s}{\lambda_p} \qquad (6)$$

Here we have $n_{o,i}$ and $n_{e,i}$ represent the ordinary and extraordinary indices of refraction at λ_i. Thus the phase matching can be achieved by varying the angle of the crystal, θ_m, with respect to the optical axis. It is also possible to tune the phase matching via temperature control. For example, the second harmonic generation of the YLF laser fundamental is optimized via temperature tuning.

Utilizing sum frequency generation as a means to time resolve luminescence is a relatively recent technique. Though a few examples arise from the 1970's[63-71] upconversion has become more widespread recently. One reason for its increasing usage

may be the advent of commercially available, stable, ultrafast laser systems. Furthermore, as the field of short pulse generation continues to advance[72], the gap between the pulse width limit and the time domain of techniques such as TCSPC widens. Increasingly, phenomena on ultrafast time scales are being explored, and corresponding advances in spectroscopic methods accompany this trend.

Two distinct configurations for luminescence upconversion exist, based on the choice between high repetition rate (low pulse power) and low repetition rate (high pulse power) lasers. This trade-off is not unique to upconversion systems, but to a greater or lesser degree, is always a consideration when designing a laser experiment. If one works in the low power regime, signal levels are small, but the experiment is averaged over millions of laser shots per second. Conversely, high power laser systems generate larger signal levels, fewer times per second. The signal averaging is typically done each shot, or group of shots, by comparison to a reference pulse. Luminescence upconversion has been demonstrated in both regimes.

Semiconductors are well suited to upconversion based on high repetition rate lasers. In these materials damage thresholds and carrier densities are considerations. The heat deposited in an ultrafast laser pulse can be significant and can lead to effects such as melting and ablation. In particular, semiconductors have been studied with MHz repetition rate systems under single photon counting conditions. Shah and coworkers have performed extensive development of luminescence upconversion spectroscopy for semiconductor experiments.[62] Their developments form the basis of the system designed and constructed for this thesis work. Shah and coworkers utilize a laser system similar to the one described above to generate picosecond pulses.[73] Furthermore, they

have employed optical fiber pulse compression to extend this technique into the femtosecond range. The first step involves pulse compression of the fundamental of a YAG laser prior to frequency doubling.[74] This compression allows the dye laser to be pumped with a 3.5 ps pulse rather than the typical 90 ps. The output of the dye laser was reduced to ~ 300 fs, and ultimately improved to ~ 100 fs resolution.[75] Furthermore, after pulse compression of the dye laser output, 65 fs resolution was achieved.[76] Extending upconversion into the femtosecond regime requires additional considerations. In particular, the use of dispersive optics in the experimental set-up will broaden the pulse width due to the group velocity dispersion.

As mentioned above, luminescence upconversion has also been applied in the low repetition rate, high power regime, primarily to processes in solution. In this case, the same density of excited states are not generated as in the solid state, so high power laser pulses can be utilized. Also, in solution phase experiments, the sample can be flowed through a cell or jet. Thus, even if the sample photo-decomposes, each laser shot probes fresh solution. An example of this type of system can be found in work by Barbara and coworkers.[77,78] They developed a 70 femtosecond upconversion spectrometer operating at 8.2 KHz. The output of a femtosecond dye laser is amplified via a copper vapor laser pumped dye laser amplifier. Typical pulse energies for this system are 2 μJ, whereas MHz repetition rate lasers produce nJ pulse energies.

Another experimental distinction between the amplified and unamplified systems involves the method of signal averaging. Multipass dye laser amplifiers introduce a fair amount of noise into the laser system. As upconversion is a nonlinear process, fluctuations in the laser pulse power will have a large effect on the signal. It is not

uncommon for the dye laser fundamental to be frequency doubled to generate the sample excitation wavelength. In this case, the final upconverted signal will be proportional to the cube of the laser intensity. Hence, it is necessary to monitor fluctuations in the laser output and normalize the upconverted signal to these changes. In the single photon counting mode, the unamplified laser is more stable, and is typically not the largest source of noise.

The development of a time resolved luminescence measurement technique with pulse width limited resolution allows processes to be probed on time scales previously inaccessible. A few examples of the application of sum frequency generation are given to demonstrate its utility as a spectroscopic tool. In the area of semiconductor physics, the ultrafast dynamics of carriers are of widespread interest, primarily due to the potential for microelectronic applications. Luminescence is an excellent probe of the energy distribution of carriers. The time evolution of the spectra yields information on the relaxation of this distribution. For example, on the picosecond time scale, luminescence upconversion has been applied to the process of intervalley scattering in InP.[73] On subpicosecond time scales, the initial thermalization of the hot distribution is probed. These studies provide information on carrier-carrier scattering, one of the shortest time scale interactions that photoexcited carriers undergo.[79,80] Another interesting area where luminescence upconversion has recently been applied is the study of carrier spin relaxation.[81-83] The initial spin distribution of photoexcited carriers is rapidly relaxed, hence these experiments require high quality materials, and measurements on ultrafast time scales. Due to advances both in semiconductor materials synthesis, such as molecular beam epitaxy (MBE), and ultrafast spectroscopy, spin relaxation in magnetic

semiconductors has been observed via luminescence polarization. In addition to the area of semiconductor dynamics, luminescence upconversion has been applied to chemical systems. The Barbara upconversion configuration described above has been used to probe solvation dynamics which occur in less than 10 picoseconds.[84,85] For example, the fluorescence spectra of coumarin in polar solvents undergoes a red shift corresponding to solvent reorientation. Fleming and coworkers have applied luminescence upconversion to fluorescence anisotropy studies in solution and also to solvation dynamics.[86-91] Tryptophan has been suggested as a probe of protein folding, and hence its luminescence as a function of orientation is of interest.

This section will conclude with a brief comparison of the merits of TCSPC and luminescence upconversion. Clearly fluorescence spectroscopy is of widespread utility, and a technique with the shortest time resolution possible can be applied to problems which are inaccessible by other methods. On the basis of time resolution, luminescence upconversion is the best technique. Furthermore, being primarily pulse width limited, it has the advantage that, once a system is built, further gains in time resolution can be achieved merely through improvements in the laser. For example, the system utilized for this thesis may be upgraded through the application of pulse compression, improving the current time resolution from 1 ps to 200 fs. With the increasing proliferation of commercial ultrafast lasers, luminescence upconversion will be applied to more problems in physical and chemical systems. In particular, the Ti:saphire laser system, with its ease of usage, ultrafast pulses (sub-100 fs) and wavelength range, will be readily adapted to sum frequency generation. The near IR and visible wavelengths are particularly

amenable to sum frequency generation, due to the ease of detecting visible and uv upconverted wavelengths.

Though luminescence upconversion is the technique of choice for ultrafast time resolution, it is more difficult to implement than TSCPS and yields worse signal to noise. Several factors make detecting luminescence with upconversion less sensitive than directly collecting luminescence with a PMT. Luminescence signal is lost from incorrect phase matching and poor overlap of the signal and probe beams. Upconversion requires more optical elements, each of which contributes to the loss of signal. Finally, even under optimal collection and overlap conditions, the inherent inefficiency of the optical process means that a small percentage of the luminescence which makes it to the nonlinear crystal will be upconverted. Hence this technique requires a relatively large signal. Direct band gap semiconductors and dye molecules are good candidates for upconversion, as they often have quantum yields of at least a few percent.

Luminescence upconversion generates a large background signal which creates experimental difficulties. The strong laser probe pulse, in addition to the upconversion process, will undergo second harmonic generation. Even when the nonlinear crystal is set to the phase matching angle for the upconverted wavelength, significant SHG occurs. Empirically, SHG was observed even when the upconverted and SHG wavelengths were separated by 50 nm. This background SHG occurs because the probe pulse is so much stronger than the fluorescence signal. Even under non-optimal conditions, the amount of SHG is significant when compared to the upconverted signal. This signal presents problems in several ways. Stray light must be filtered from the optical path. A combination of cut glass filters and a monochromator were utilized to remove stray light.

Of course, this selectivity also diminishes the desired signal to some extent. Ultimately, interference from SHG will limit how close to the excitation wavelength one can detect. This constraint means that an experiment with near resonant excitation and detection is not feasible. For example, this situation may arise in semiconductor spin experiments, when exciting preferentially from the heavy hole versus light hole sub-band. Freeman and coworkers developed a two dye laser system to perform upconversion under these conditions.[92]

By comparison, TCSPC has essentially no background signal. Microchannel plates for visible and ultraviolet detection have very low dark count rates, < 50 cps. Furthermore, by synchronizing the signal detection to the laser pulse within a narrow time window (typically 20 ns), even lower background rates, < 5 cps, are achieved. As a result, the largest source of noise arises from the photon counting statistics. Therefore, data collection can be continued until thousand of events are detected and the desired signal to noise levels are achieved. In general, TCSPC produces excellent signal-to-noise quite easily. Moreover, drifts with time of the signal detection or laser power do not show up in the single photon distribution. Whereas, in luminescence upconversion, the data must be collected in an amount of time over which the laser intensity is constant, since the signal is directly proportional to the laser intensity. Finally, TCSPC can be applied to problems with much lower signal levels than luminescence upconversion.

2. Details of Our Picosecond Luminescence Upconversion Spectrometer

In this section, the particular details of our spectrometer will be discussed. The diagram of the spectrometer is given in Figure 7. Many experimental details are included

Figure 7. Picosecond luminescence upconversion spectrometer. In these experiments, the dye laser is operated in the dual-jet mode, to produce ~ 1 ps pulses at 590 nm and 3.8 MHz. A portion of this visible beam is sent through a variable path length (TRANSLATION STAGE), and focused onto the face of the semiconductor(XTAL). The luminescence is collected and recombined with the remainder of the laser pulse train and focused into a nonlinear crystal (BBO). The overlap inside the BBO is aided by CCD camera. The ultraviolet upconverted light is then passed to the monochromator (MC) and microchannel plate (MCP), as in the TCSPC experiment. (See Figure 3.) Notice the similarity to the TCSPC set-up. However, here, the time resolution is determined by the variable path length of the laser pulse and not the microchannel plate.

PICOSECOND UPCONVERSION SPECTROMETER

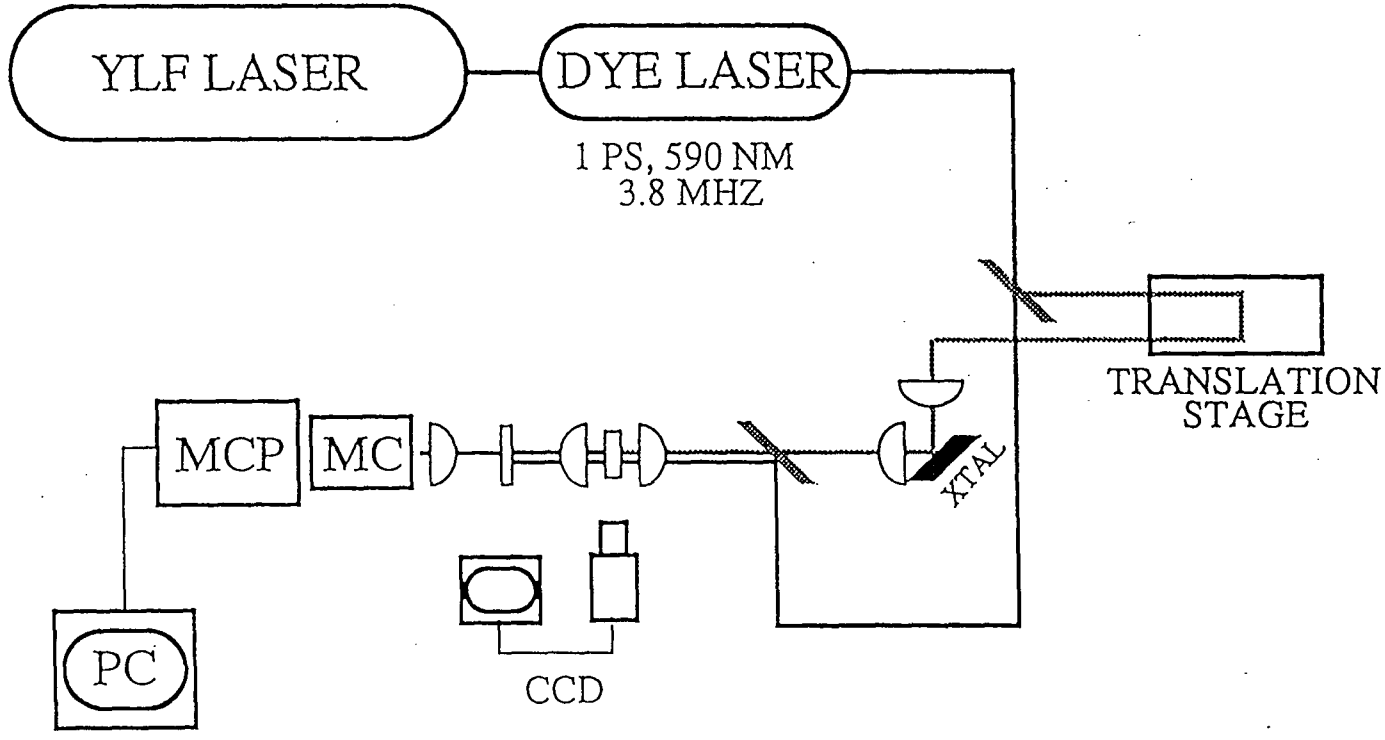

in this Section, as this information may prove useful in the future design of an upconversion spectrometer. The laser system which is utilized in this spectrometer is essentially the same as that for photon counting. That is, the mode-locked Coherent YLF laser is used to pump the Coherent 700 series dye laser. The dye laser is operated in the two-jet configuration, and cavity dumped at 3.8 MHz. The dye combination utilized was typically R6G and DODCI. Typical output consisted of 1 ps pulses at 590 nm with an average power of 250 mw.

The dye laser output was directed to a variable beamsplitter which was adjusted to transmit a fraction of the main beam, ~10%, and reflect the remainder. The transmitted beam was passed to a variable delay path consisting of a pair of mirrors defining a path parallel to the motion of the translation stage. This translation stage was a Klinger model MT160.150 with a computer controlled, programmable stepper motor controller, model CC1.1. The path length of the stage was 150 mm, and it could be stepped in increments of 10 μm with the CC1.1 controller. With an alternate controller, the stage could be stepped in 1 μm increments, which corresponds to a time-resolution of 3 fs. Hence, the stage is capable of far greater time resolution than was required in this experiment.

The beam exiting the translation stage was focused onto the semiconductor sample with a 5-cm focal length lens (CVI plcx25.4/18.0, uv-grade). The lens was mounted in a NRC Variable Lens Holder (LFM1), which can be rotated to change the distance of the lens to the sample, creating a tighter or more diffuse focus. The excitation beam was focused onto the semiconductor sample at an oblique angle to the surface, typically 45 degrees or less. The sample was mounted on the end of a glass rod with epoxy and held in an NRC post holder. The semiconductor luminescence is collected

from the front side of the sample. If the residual, scattered excite beam is blocked with a colored filter, the luminescence can be detected by eye as a bright spot on the surface of the semiconductor.

The sample fluorescence was collected with a NRC microscope objective, with 20X amplification, and a working distance of 1.8 mm from the end of the optic. The upconverted signal was extremely sensitive to changes in luminescence collection efficiency. Hence, the alignment of this optic was highly sensitive. To optimize the luminescence collected, several degrees of freedom were added to this optic for adjustment. The microscope objective was mounted in a holder with adjustment in the two planes perpendicular to the optical axis. The mount was suspended from above on a bracket attached to a large post holder. The bracket was mounted on a translation stage which gave height adjustment (perpendicular to the table top). The large post holder was mounted on two translation stages with horizontal motion, both along and perpendicular to the optical axis. In particular, these last two adjustments were critical for the fluorescence collection efficiency. The collected luminescence emerged from the microscope objective in a collimated beam. This beam was directed along the predefined, upconversion optical axis.

The portion of the laser pulse train which was reflected from the front side of the variable beamsplitter served as the upconversion gating pulse. This beam traversed a fixed path and was recombined with the sample fluorescence by a custom made dichroic optic (CVI). These optics were designed to reflect the gating pulse and transmit the semiconductor luminescence. After the dicroic optic, the gating pulse is collinear with

the luminescence. The dichroic beamsplitter is mounted in a mirror holder with adjustments perpendicular to the optical path.

These two beams are focused into the nonlinear crystal, a 2 mm BBO crystal from CSK. A 5X microscope objective serves as the optic to focus into the BBO. The microscope objective is mounted in an objective mount with adjustments. The assembly is mounted onto a translation stage with motion along the optical axis. This motion serves to focus more or less tightly into the BBO. The BBO is mounted in a mirror mount, also allowing tilt and angular adjustment. The angular motion of the BBO is critical for phase matching purposes. A lens was placed on the exit side of the BBO to roughly recollimate the exiting upconversion signal. This optic was a uv grade, CVI plcx25.4/25.8 lens, mounted in a lens holder and onto a translation stage with motion parallel to the optical axis.

At this point along the optical path, filters were utilized to removed stray light. A 3 mm thick, UG11 filter serves to remove remaining visible light due to the laser fundamental, i.e., the gating pulse. UV cut off filters were used to help remove SHG which interferes with the upconverted signal. Typically a 3 mm WG320 filter was utilized. A Melles Griot uv grade condenser (01-CMP-119) served as the optic to focus the ultraviolet upconverted photons onto the entrance slit of the monochromator. The condenser was mounted on a translation stage with motion along the optical axis. This motion was used to change the focus onto the monochromator slit. The slits utilized were typically .25 mm, which provide ~ 4 nm resolution in the uv wavelength range of the upconverted light.

The monochromator was mounted on the front of the MCP housing, as in the TCSPC experiments. The rest of the electronic detection of the signal was similar to the TCSPC setup. The equipment was available to detect the upconverted photons in the "time-correlated" mode, where the upconverted luminescence is synchronized to the laser pulse train. This configuration will reduce dark counts, if they are a problem. Typically, signal levels were such that this synchronization was not necessary. The SCA output of the Ortec discriminator was fed into a Fast/Slow Logic interface to generate the pulses sent to the counter/timer chip. The counter/timer was an IOTech Power 488CT which was a plug-in module for a 486 PC. This board also served as the IEEE-488.2 interface for the translation stage controller.

3. Details of Operation for Picosecond Luminescence Upconversion

The purpose of this section is to describe some of the practical aspects of implementing luminescence upconversion.

a. Alignment of Translation Stage

In the spectrometer utilized in this work, the variable path length was incorporated into the excite portion of the laser beam. In this case, the sample fluorescence is initiated at different times, which correspond to different stage positions. The probe beam follows a fixed path and intersects the luminescence in the upconversion crystal at fixed time and position. It is not difficult to roughly align the laser path along the direction of motion of the stage. An iris was utilized to reproducibly position the incoming beam along a path that was initially carefully chosen to be parallel to the motion of the stage. Two mirrors at 45° to the laser determine the exit path of the beam and also provide two independent

adjusts. Another iris was placed to position the exit beam. By iteration, the two mirrors were adjusted at the two extremes of the stage motion to center the beam on the iris. Thus, in principle, the output beam is not "walking" or "steering" as a function of the stage position. However, in practice, the sample luminescence was extremely sensitive to the path of the excite laser. Even if the stage was aligned such that, by eye, no motion in the beam is detected, the luminescence counts may not be constant.

This sensitivity to position of the excite beam arises from the variation in collection efficiency if the excite is moved. This conclusion agrees also with the observation of the signal sensitivity on the optic utilized to collect the luminescence. (See discussion below.) Hence, one has to take great care in the alignment of the outgoing beam, to make sure that the stage does not walk off the luminescence from its optimal position. After roughly aligning the stage position by eye, the alignment was optimized by looking directly at the luminescence signal itself and carefully checking that the signal did not change as a function of stage position. The "flatness" of the luminescence signal over the motion of the stage was checked before and after a set of upconversion experiments. Sometimes, there was a few percent drift that could not be eliminated, but gross drifts in the signal were eliminated. Furthermore, this background luminescence scan could be saved for future correction to the data, if necessary.

In retrospect, it is recommended that the stage delay be inserted in the probe arm, and not the excite beam. Initially, it was thought that the position of the probe beam striking the BBO would be have the largest effect on upconversion efficiency. The semiconductor luminescence efficiency is not very sensitive to the position of the excite beam, and that was the initial consideration. But the collection efficiency is more

sensitive, and this factor is experimentally more difficult to control than the overlap of the probe beam in the upconversion crystal.

b. Collection Efficiency of Semiconductor Luminescence

As mentioned above, the luminescence detected from the sample was extremely sensitive to the positioning of the collection optic. The experimental geometry always involved collecting luminescence from the same side of the semiconductor as the excite. It was determined that a microscope objective worked better than a low f-number lens for collecting luminescence, for two reasons. In order to focus tightly into the upconversion crystal, a smaller diameter, collimated beam is desired. The microscope objective produces a 7 mm diameter beam. Secondly, the working distance was 1.9 mm, which means the tip of the objective is close to the excitation spot of the sample. This placement helps to collect a wide solid angle of luminescence. Shah and coworkers utilize a Cassagranian for luminescence collection. This optic is nondispersive, and will not broaden time resolution, as required for femtosecond applications.

The positioning of the microscope objective was the most crucial adjustment for maximizing upconverted signal. The optic was mounted with several degrees of freedom, as described in the previous section. The most important ones were the distance from the lens to the sample, i.e. the focal length, and also the motion perpendicular to the optical axis in the horizontal plane. The collection optic should be mounted on translation stages with fine adjustments for these directions.

c. Collinear Geometry

The experimental design can incorporate collinear geometry for the luminescence and probe, or the two beams can intersect at an angle. The easiest configuration to

construct is the collinear geometry. For a tight focus, it is hard to get two sets of steering and focusing optics near the nonlinear crystal. In picosecond experiments, a thicker nonlinear crystal can be used. In this case, the overlap can be maximized with a collinear geometry. The drawback is the large second harmonic signal which emerges in the same direction as the upconverted signal. If the upconverted and SHG wavelengths are widely separated, then efficient separation with a monochromator and/or prisms is feasible. For example, upconversion experiments with infrared wavelengths and a visible probe are good candidates for collinear geometry. These experiments, with the upconverted and SHG wavelengths separated often by only ~ 15 nm, are barely feasible.

d. Spatially Overlapping Luminescence and Probe

In an upconversion experiment, one of the difficulties lies in spatially overlapping the sample luminescence with the probe beam inside the nonlinear crystal. Irises were utilized to define the optical axis for upconversion. The luminescence was strong enough to be visible by eye (in a darkened room), and the rough alignment could be done with the irises. The much stronger probe beam was passed along the same axis. The first step in overlapping the beams was done in this manner. Since there is no scattered light from the smooth upconversion crystal, it is not possible to see by eye exactly where the two beams are focused. The next adjustment could be achieved by looking at scattered light off of an index card placed right before and after the BBO, and trying to move the two beams until overlapped. The luminescence is usually strong enough to see this way, the probe beam needs to be attenuated with an (at least) OD4 filter to be of comparable intensity. This procedure helps in that each beam can be blocked in turn, and the two can be iterated closer to each other. If the luminescence signal was easily visible when

scattered from an index card, then it was usually possible to overlap the beams in this way. Once any signal counts are detected, then the position of the beams are optimized by monitoring the upconverted signal count rate.

For signals that could not be overlapped by eye, a CCD camera was required. The probe beam had to be attenuated by OD4 or more, in order not to swamp the detector, and also such that the two beams were comparable in size. A mirror was placed behind the BBO crystal and the light was directed into the detector. In this manner, the luminescence spot could be easily seen with the camera.

e. Finding First Signal and Measuring t=0

Finding signal in an upconversion experiment is difficult initially, because the beams must be spatially and temporally overlapped and phase matched, or there is no signal at all. In practice, the most difficult is the spatial overlap, and the previous section discusses this procedure. The temporal overlap was not too difficult in the case of a picosecond experiment. The overlap can be estimated to within a few centimeters by measuring the path length. The stage is then scanned over this region when looking for signal. After the t=0 is established, it typically did not move significantly for subsequent experiments.

The tunability of the dye laser provides a good trick for phase matching. The laser was set to the wavelength whose second harmonic frequency was the desired upconversion frequency. The BBO angular position was then adjusted to optimize phase matching for this frequency. Even if the incoming direction of the beams in the actual experiment varied slightly, this prepositioning was usually close to the optimal angle. In practice, it was found that BBO possesses a generous acceptance angle at the wavelengths

detected (~ 310 nm). The bandwidth was limited to 5 nm in the uv by the monochromator slits, not by the acceptance angle of the BBO. As the detection wavelength was varied, the BBO angular setting had to be optimized, but there was overlap in the wavelengths generated at each setting. This large acceptance angle is also one of the reasons the second harmonic generation is so efficient. That result is a negative consequence of the easy phase matching.

The t=0 was found by scattering visible light off of the semiconductor front surface, collecting it, and upconverting it with the remaining laser light, as in an upconversion experiment. This auto-correlation of the laser pulse with itself serves as the instrument response of the spectrometer as well as defining the absolute t=0. In this case, the "upconverted" signal is also the same wavelength as the SHG, so the detected signal is a small change in the background SHG signal, which remains constants with stage position.

IV. Diffusion in a Band Gap Gradient

A. Graded CdS_xSe_{1-x} Semiconductors

Graded samples of n-CdS_xSe_{1-x} have been shown to exhibit color-coded photoluminescence (PL) that permits identification of the spatial origin of e^--h^+ pair recombination in continuous illumination experiments.[28,29] The observed luminescence is derived from the band edge emission characteristic of the alloy composition comprising the graded zone. (See Equation 1 in Section II.) Because the emission wavelength is related to the composition, which in turn is related to the distance away from the surface into the bulk, these graded solids are ideally suited for direct study of the carrier dynamics. Recombination of e^--h^+ pairs at various depths beyond the near-surface region where they are first created can be temporally resolved and thus give information on the diffusion times from the surface to the bulk. Figure 8 illustrates the graded CdSe/S diffusion experiment.

The experimental details are given in Section III. Briefly, the graded CdS_xSe_{1-x} samples have ~ 1-μm thick graded regions. For CdSe/S, the graded zone comprises virtually all of the alloy compositions, whereas for CdS/Se, the composition varies from ~ x=.2 at the surface to x=1 for the substrate. Sample excitation using a picosecond laser system at 315 nm creates a nonequilibrium distribution of e^--h^+ pairs with a density of ~ 10^{17} cm^{-3}. At this excitation wavelength the incident light is estimated to be absorbed within ~ 0.1 μm of the surface.[93,94] The temporal decay of the luminescence at a given wavelength is measured by using time-correlated single-photon counting techniques.

Figure 8. Graded $CdSe_xSe_{1-x}$ experiment. Electron-hole pairs are generated in the S-rich surface region of the CdSe/S graded semiconductor. The nonequilibrium distribution diffuses under the influence of both concentration and band gap gradients. These gradients drive the carriers towards the bulk, or CdSe substrate. At various depths, the e^--h^+ pairs radiatively recombine and emit luminescence at wavelengths characteristic of the composition at that position. In this manner, the diffusion process is temporally resolved.

Graded CdS_xSe_{1-x} Semiconductor

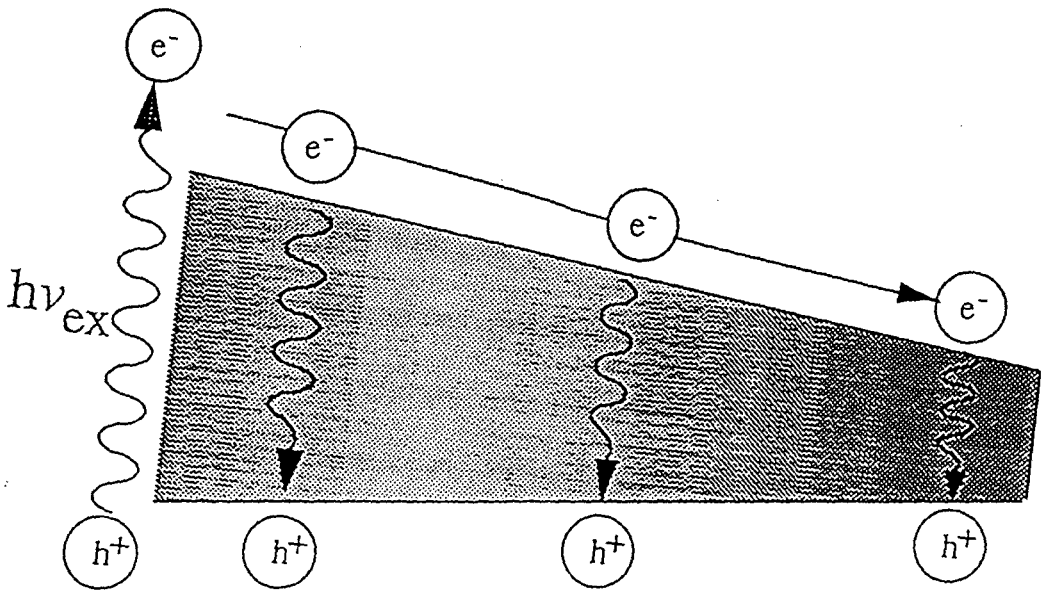

SURFACE —— 10,000 Å —— BULK

CdS

$E_g = 2.4$ eV

CdSe

$E_g = 1.7$ eV

In these experiments, the initially narrow distribution of e^--h^+ pairs is created in the near surface region. We expect these carriers to diffuse from the surface into the bulk under the influence of both concentration and band gap gradients as:

$$i = -D\frac{dn}{dx} - \frac{Dn}{kT}\frac{dE}{dx} \qquad (7)$$

where i is the particle current, D the diffusion constant, n the number of carriers, x the position, T the temperature, and E the conduction (or valence) band edge energy. The first term is the standard Fick's diffusion, and the second term indicates transport to lower band edge regions. In the CdSe/S material, both gradients favor diffusion of carriers from the surface towards the substrate. In the case of CdS/Se, the transport of particles into the bulk is opposed to the potential gradient.

These graded semiconductors provide a good model system for studying e^--h^+ pair transport. However, it is not straightforward to map the observed trends into position and time-dependent equations (diffusion and continuity equations) for the number of carriers. Equation 7 represents transport in a graded semiconductor in the special case of doping to eliminate space charge (i.e., internal electric fields).[95] In the experimental studies presented here, with arbitrary doping profile, it is not clear what effects space charge regions have on carrier dynamics. However, if these effects were extremely important, carriers would probably not reach the deepest regions, since internal electric fields move electrons and holes in opposite directions. The transport mechanisms described by Equation 7 yield particle currents in the same direction for both electrons and holes and therefore can account for smooth trends in the characteristic decay times and the appearance of carriers in the deepest regions. A further complication involves

specifying a position-dependent recombination rate that couples continuity equations for the electron and hole populations.

Data on the graded CdSe/S sample are illustrated in Figure 9. Incident excitation is absorbed in CdS and S-rich alloy strata ($x \geq 0.7$). The decay functions have 1/e time constants of ~ 100 to 400 ps. Thus, the diffusion process is occurring on a time scale that is competitive with characteristic band-to-band recombination lifetimes for direct band gap semiconductors.[96] The observed decays, however, yield information about transport, rather than merely reflecting differences in intrinsic lifetimes of the materials comprising the graded region. This conclusion is supported by extending the study to CdS_xSe_{1-x} materials with the opposite composition gradient. These results, as discussed below, demonstrate that the1/e decay constants are not the same at a given wavelength for the two materials, as they would be if only the lifetime were being measured. Instead, the decays show a dependence on factors such as band gap gradient and distance from initial excitation.

This CdSe/S experiment represents a simple example of Equation 7, as the band gap and concentration gradients act on carriers in the same direction, into the bulk. The data in Fig. 9 are in general agreement with this picture. First, the luminescence spans the entire spectral range of 500 to 700 nm, representing the full composition range of $0 \leq x \leq 1$. Clearly diffusion from the near surface region into the bulk occurs on a time scale competitive with the intrinsic e^--h^+ pair lifetime. Furthermore, as observed in Figure 9A, the 1/e decay constant increases smoothly from 500 nm ($x = 1.0$) to 620 nm ($x = .50$). This trend is consistent with the picture of carrier diffusion from the surface into the bulk.

Figure 9. Time resolved luminescence from CdSe/S graded semiconductor. (A) The luminescence time constants for 500-620 nm become longer at longer wavelengths, corresponding to increasing distance from initial excitation. (B) The 620-720 nm region demonstrates a reversal of the previous trend.

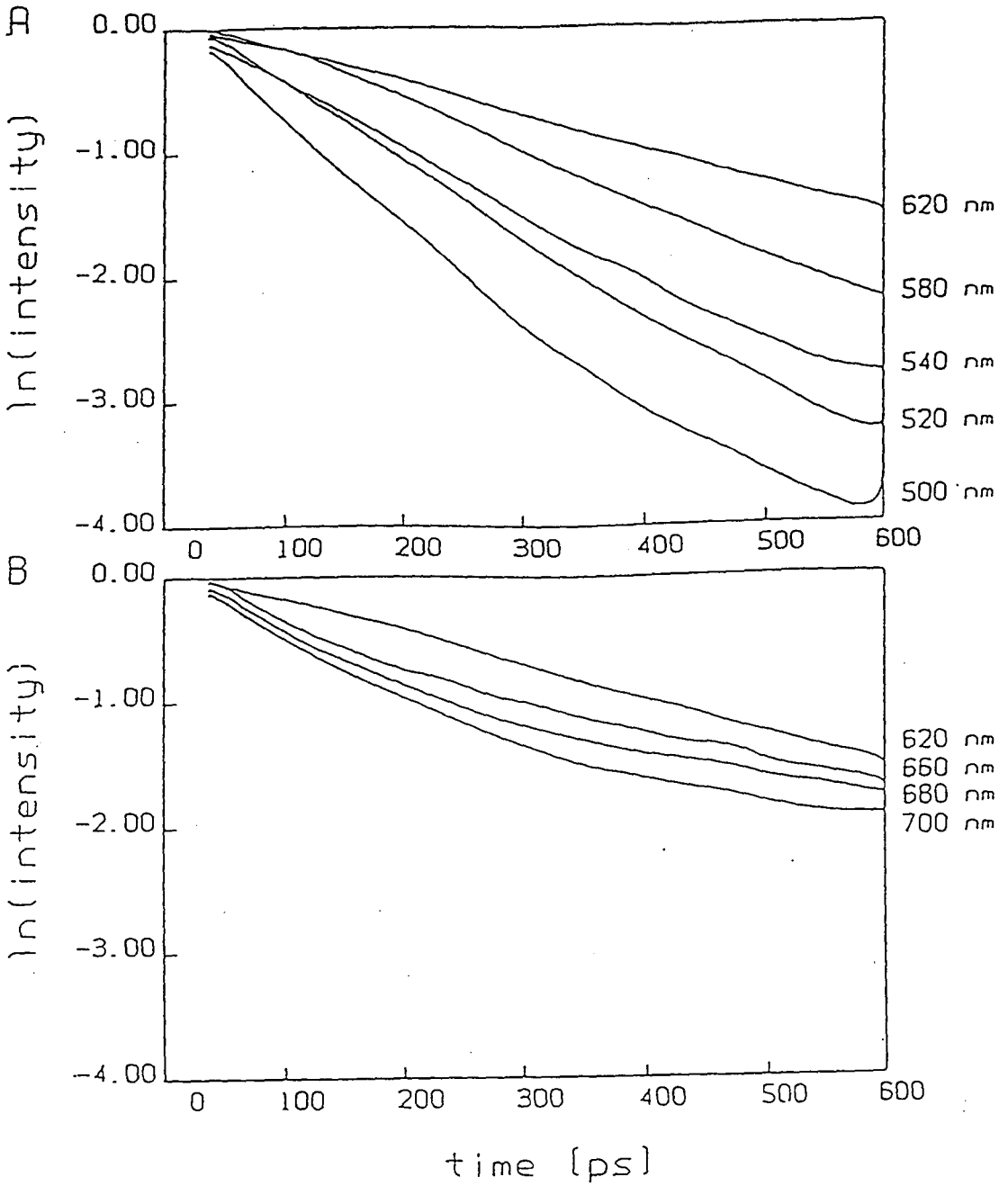
A
0.00
-1.00
-2.00
-3.00
-4.00
ln(intensity)
0
100
200
300
400
500
600
620 nm
580 nm
540 nm
520 nm
500 nm
B
0.00
-1.00
-2.00
-3.00
-4.00
ln(intensity)
0
100
200
300
400
500
600
620 nm
660 nm
680 nm
700 nm
time [ps]

An estimate of the ambipolar mobility can be determined from this difference in decay constants, the potential drop, and the depth profile over this region:

$$\mu = \frac{v}{E/cm} \approx \frac{\frac{5000\text{Å}}{300ps}}{\frac{0.35V}{5000\text{Å}}} \approx \frac{24cm^2}{Vs} \qquad (8)$$

This value is in accord with the mobilities for CdS and CdSe materials.[97]

The dual processes of diffusion in band gap and concentration gradients are not sufficient to explain all of the CdSe/S features. The time decays in the 620 to 700 nm region, Figure 9B, which represent the region from about midway through the gradient (x = .50) to the substrate (x = 0), are qualitatively different. The opposite trend in 1/e time constants (t) is observed, the t's become shorter at longer wavelengths. Also, the spread in t's is small compared to the span in the initial region. These apparently anomalous features can be qualitatively understood, through the subsequent studies on homogeneous crystals, which are discussed in the next subsection.

The second graded semiconductor, CdS/Se, is a somewhat more complicated test of Equation 7, as the band gap increases with distance from the surface. In this case, the concentration and band gap gradients oppose each other. Furthermore, the processes of self-absorption and reemission may occur in this material. These results are shown in Figure 10. Despite the added complexity, this data demonstrates several important results. If the graded semiconductor data were dominated by the intrinsic lifetimes of the e^--h^+ pairs at the given compositions, then the wavelength dependence for the two samples would be identical. As this result is not observed, the data clearly contains

Figure 10. Time resolved luminescence from graded CdS/Se semiconductor. (A) The luminescence time constants become longer at shorter wavelengths, corresponding to increasing distance from the initial excitation. The data demonstrate that e^--h^+ pairs reach the substrate, even though this appearance requires diffusion against the potential gradient. The concentration gradient is the driving force. (B) The 620-740 nm region reflects a reversal of the previous trend. This near surface region may reflect self-absorption and reemission effects.

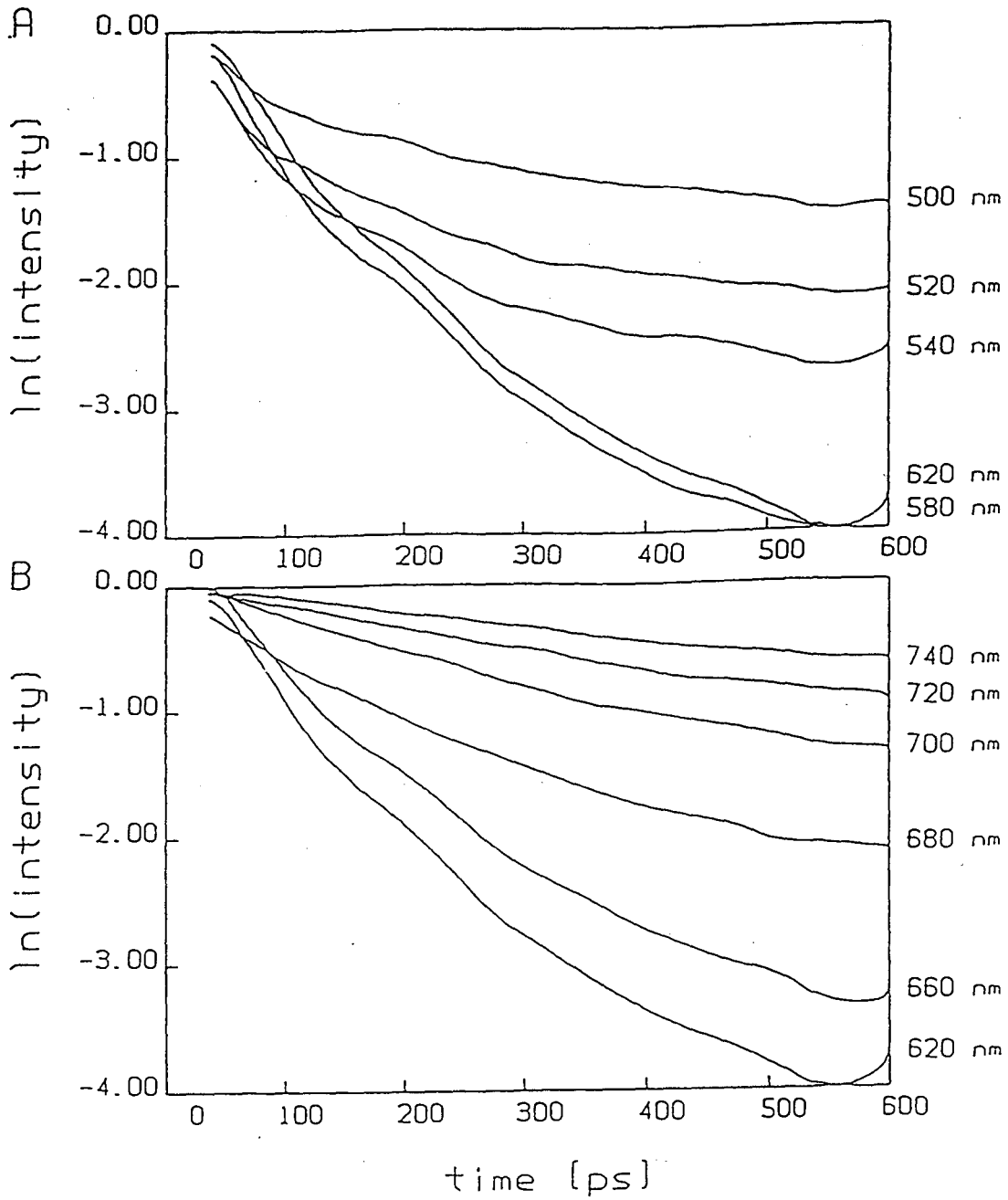
A
0.00
-1.00
-2.00
-3.00
-4.00
ln(intensity)
500 nm
520 nm
540 nm
620 nm
580 nm
0
100
200
300
400
500
600
B
0.00
-1.00
-2.00
-3.00
-4.00
ln(intensity)
740 nm
720 nm
700 nm
680 nm
660 nm
620 nm
0
100
200
300
400
500
600
time [ps]

information about the dynamics, as well as the lifetimes. Secondly, it is apparent from the data that diffusion against the potential gradient occurs, as luminescence is observed even at the 500 nm wavelength characteristic of the CdS substrate. The concentration gradient is the driving force, in this case. It is sufficient to drive the e^--h^+ pair transport up a band gap gradient of at least ~ 0.35 eV (assuming significant absorption occurs to the region of roughly $CdS_{.50}Se_{.50}$ composition.)

An interesting feature of this data is that the trends in time constants are completely reversed with respect to the CdSe/S results. From 620 to 500 nm, shown in Figure 10A, representing x = .5 to x = 1, the lifetimes increase with decreasing wavelength, or increasing depth into the sample. However, in the region from 620 to 740 nm, Figure 10B, the reverse trend exists, where an increase in *t* does not correspond to an increasing depth. Two processes may explain the latter result. After the concentration gradient has decreased, diffusion back down the potential gradient may become more important. Also, strong self-absorption and reemission in the smaller band gap, near surface region, would yield the observed trend. As these mechanisms are not possible in the CdSe/S crystal, the processes in the two samples are not completely complementary. However, in both cases, the turnover in lifetime trend occurs at 620 nm, characteristic of the x = .50 composition.

The time evolution of the spectra for the graded materials also serves to demonstrate the diffusion of e^--h^+ pairs into the bulk substrate. "Gated" photoluminescence spectra are given in Figure 11. These spectra reflect only events that occur in a given time window of 400 ps. As the window is shifted in time, after the initial excitation, the resulting spectra show an increase in relative intensity at wavelengths

Figure 11. Gated CdS_XSe_{1-X} Photoluminescence. (A) The gated spectrum of CdSe/S, collected after 1 ns, demonstrates a relative shift to longer wavelengths, corresponding to the appearance of e^--h^+ pairs at regions removed from the initial excitation. (B) The gated spectrum for CdS/Se shifts to shorter wavelengths characteristic of the more S-rich compositions.

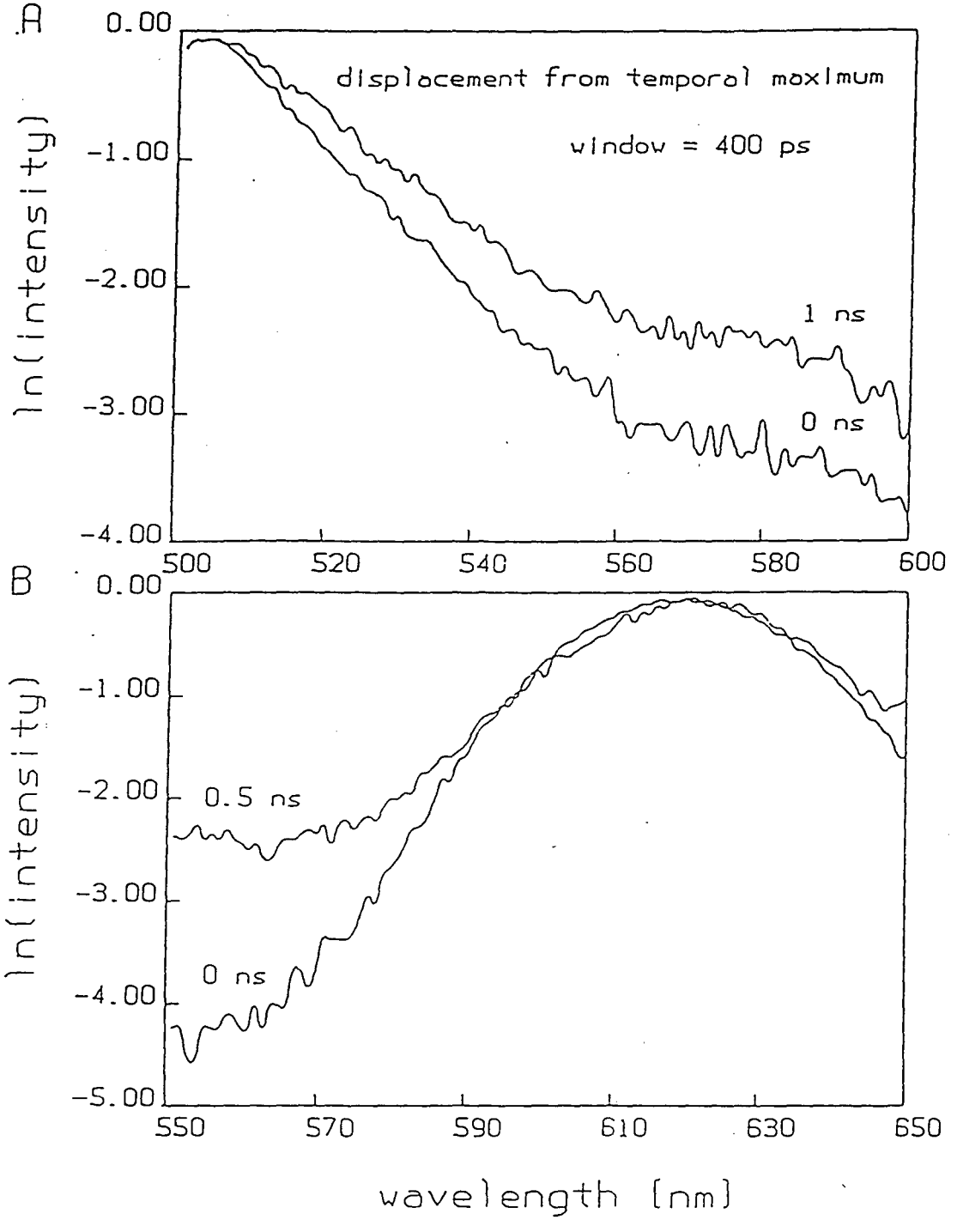
A
0.00
-1.00
-2.00
-3.00
-4.00
ln(intensity)
displacement from temporal maximum
window = 400 ps
1 ns
0 ns
500
520
540
560
580
600
B
0.00
-1.00
-2.00
-3.00
-4.00
-5.00
ln(intensity)
0.5 ns
0 ns
550
570
590
610
630
650
wavelength [nm]

characteristic of the bulk. In Figure 11A, the spectrum shifts to longer wavelengths in the CdSe/S graded sample with the CdSe substrate. In Figure 11B, the CdS/Se material shows a relative increase in the shorter wavelength emission characteristic of CdS.

To summarize this subsection, the graded CdS_XSe_{1-X} semiconductors provide an interesting system to probe the effects of band gap distortion over a macroscopic distance on the dynamics of excess e^--h^+ pairs. The luminescence decay functions for samples with both increasing and decreasing band gap reflect diffusion in concentration and band gap gradients as expected, although some features cannot be explained solely by these two mechanisms. In particular, both CdSe/S and CdS/Se samples possess a turnover in the smooth trend of time constant versus distance around the $CdS_{.50}Se_{.50}$ composition. This effect may be described as a "bottleneck" in the carrier mobility through the region with this composition. Hence, the next subsection will examine the behavior of carriers in a series of samples with particular composition "x".

B. Homogeneous CdS_XSe_{1-X} Semiconductors

As discussed in the previous subsection, the graded semiconductors are materials in which the composition, and hence band gap energy, vary smoothly as a function of depth. The samples change from CdS to CdSe over the distance of approximately one micron. This thickness is large relative to the lattice constants, such that at any given position in the graded region, the environment may be described as a "slab" of semiconductor with a particular uniform composition. Diffusion in band gap and concentration gradients is sufficient to describe many aspects of the graded

semiconductor, time resolved luminescence. Thus, in the simplest picture, the influence on the e^--h^+ pair transport in a particular "slab" of the graded semiconductor can be described by an average property such as the band gap energy. However, not all aspects of the time resolved data can be understood with this description. Several additional considerations are obvious. For example, when the intrinsic lifetime of a particular composition is competitive with the diffusion into and out of that composition, the decay profile will reflect both processes. Furthermore, as previously mentioned, a given composition is comprised of a distribution of S versus Se lattice sites. If the carriers were strongly influenced by the local environment, a significant wavelength dependence of the intrinsic lifetime may be present. Since the luminescence at a given wavelength reflects the lifetime of all transitions at that energy, the decay function would consist of a distribution of lifetimes.

Thus, in order to obtain a more complete description of diffusion in the inhomogeneous semiconductors, a thorough wavelength dependence of the time resolved luminescence was performed on a set of homogeneous semiconductors representative of the full composition range. The samples studied were x = 0, .25, .50, .75, and 1. The steady state luminescence spectra are narrowly peaked , FWHM ~ 30 nm, approximately around the wavelength given by Equation 1. The time resolved measurements were performed via time-correlated single photon counting. The decay functions from the peak intensity of each sample are compared in Figure 12. The data exhibit a strong lifetime dependence on composition. The CdS and CdSe materials are both equally fast. The $CdS_{.50}Se_{.50}$ sample possesses the longest decay constant and the $CdS_{.25}Se_{.75}$ and $CdS_{.75}Se_{.25}$ are intermediate.

FIGURE 12. Homogeneous CdS_xSe_{1-x} time resolved luminescence as a function of composition. The luminescence decay functions are presented for the peak emission wavelengths of five samples, x= 0, .25, .50, .75, and 1. The time constants demonstrate a strong dependence on composition. The longer lifetime for $CdS_{.50}Se_{.50}$ relative to the binary compositions reflects increased radiative recombination from localized states.

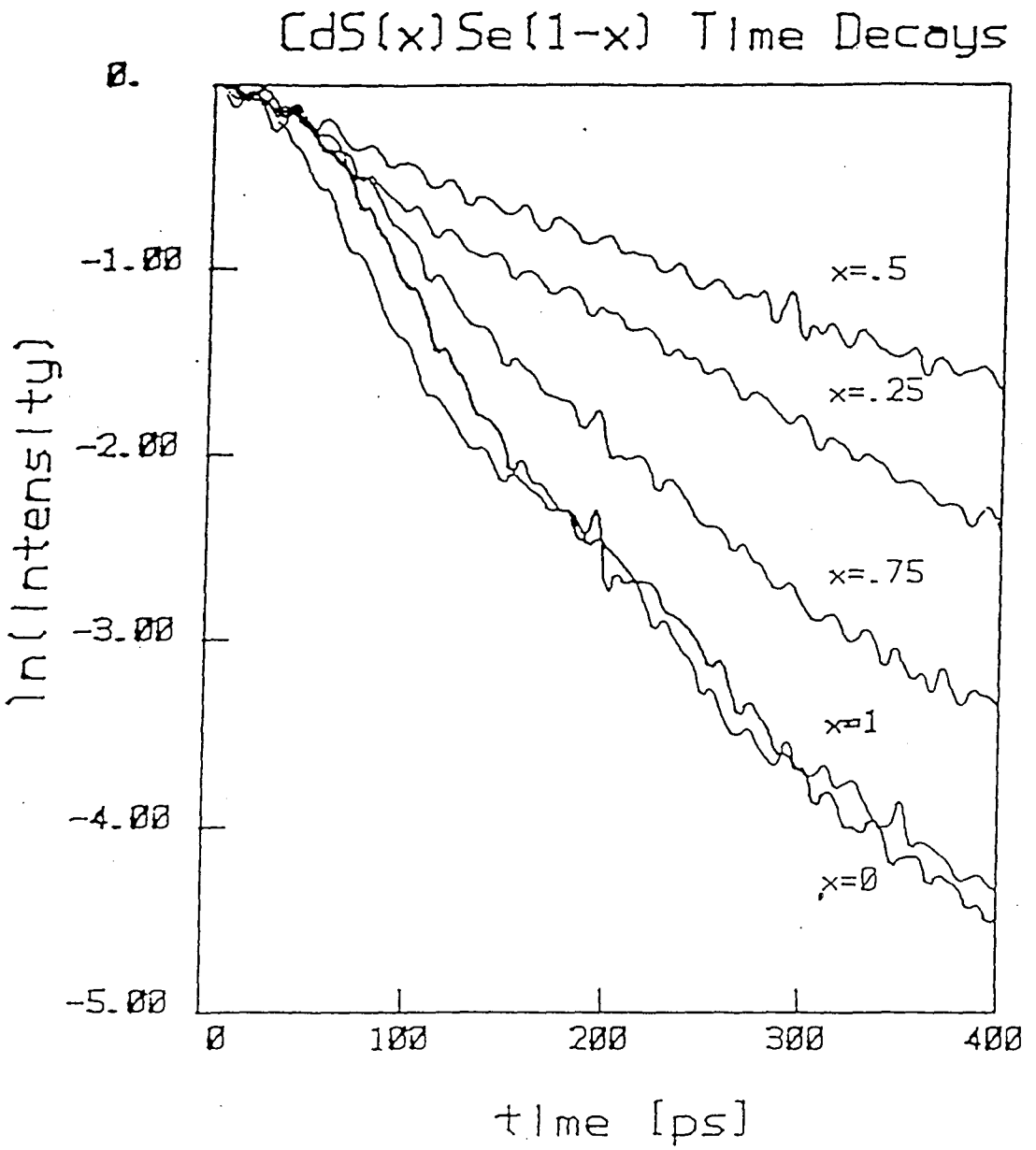
CdS(x)Se(1-x) Time Decays
0.
-1.00
-2.00
-3.00
-4.00
-5.00
ln(Intensity)
x=.5
x=.25
x=.75
x=1
x=0
0
100
200
300
400
time [ps]

One feature of this data which is of immediate interest is the longer lifetime of the $CdS_{.50}Se_{.50}$ material. This composition is approximately the same as the region in the graded materials in which the "bottleneck" occurs. These two experimental results support a particular explanation. Specifically, these results are consistent with the presence of disorder induced localization. That is, the random potential fluctuations induced by the S versus Se substitution create localized states. The depth of the localization potential is dependent upon the degree of disorder.[98] Thus localization will not occur in the pure binary semiconductors, and may be predicted to be maximized near x = .50, the most highly disordered material. More precisely, the maximum localization potential is shifted toward larger "x" values. The phenomena of disorder induced localization in alloy semiconductors will be discussed in more detail in the following Section.

The major consequence of localization, in this experiment, is the reduction of carrier encounters with nonradiative traps. Thus localization will increase the measured luminescence lifetime. The agreement between the decay times for the data in Figure 12 and the amount of disorder demonstrates that the time resolved luminescence of CdS_xSe_{1-x} alloys is sensitive to the microscopic details of the material. The main decay mechanism is nonradiative in these alloys. However, it appears that even a fraction of time spent in localized states may strongly influence the observed decay functions.

In addition to the lifetime dependence on composition, the lifetime as a function of the wavelength spread within each sample was measured. Typically, the luminescence was measured at the peak wavelength of the luminescence spectra, and also at two scans at 10 nm intervals to each side of the maxima. In general, no wavelength dependence of

the decay functions was found within a given crystal. A typical spread within a data set is shown in Figure 13 for $CdS_{.50}Se_{.50}$. Thus for a given composition, a single effective time constant is sufficient to characterize the sample.

One limit to the data obtained in these experiments on the homogeneous CdS_xSe_{1-x} crystals, is the amount of quantitative information which can be extracted. The time constants in Figure 12 are all extremely fast (~100 to 250 ps), and in the cases of CdS and CdSe, are competitive with the TCSPC instrument function. In practice, we find that this fast decay places limits on our ability to model and fit the data. Clearly, the main decay mechanism for these materials is nonradiative. Conditions which change, for example, the surface conditions of the materials affect the measured time constants. The time resolved luminescence measurements on these materials were performed under material conditions which were held as similar as possible. All of these homogeneous materials were "as purchased" from Cleveland Crystals. They possess a mechanical polish, which is reasonably the explanation for the high degree of nonradiative relaxation. However, the qualitative results of these experiments are valid, including the dependence of lifetime on composition and the ordering as a function of degree of alloy disorder. These initial experiments serve as a rough measure of the influence of the lifetime at each composition on the observed dynamics in the graded CdS_xSe_{1-x} materials.

Figure 13. Wavelength dependence for homogeneous CdS_xSe_{1-x}. The time resolved luminescence for $CdS_{.50}Se_{.50}$ at five wavelengths spanning a 40 nm range reflects no significant difference in time constants. A similar result was obtained for the wavelength dependence of all five compositions probed. For the $CdS_{.50}Se_{.50}$ data, also note the significant curvature in the ln plot, reflecting nonexponential decay dynamics.

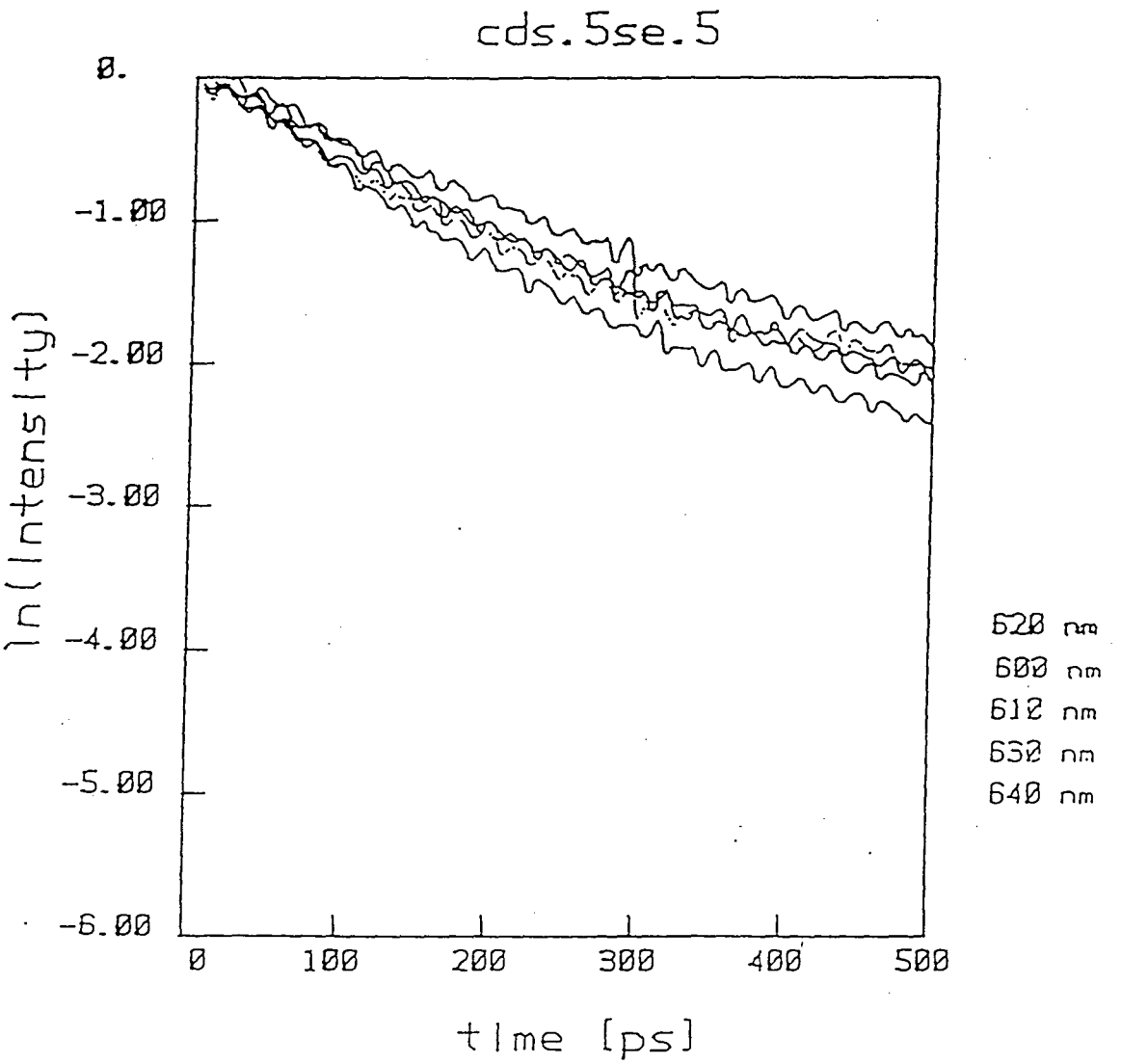
cds.5se.5
0.
-1.00
-2.00
-3.00
-4.00
-5.00
-6.00
ln(Intensity)
0
100
200
300
400
500
time [ps]
620 nm
600 nm
612 nm
632 nm
640 nm

C. Summary

The picosecond time resolved luminescence of the CdSxSe1-x semiconductor system was measured for inhomogeneously graded samples, as well as for single composition homogeneous crystals. The CdSe/S graded semiconductor exhibits strong wavelength dependent decay times, which reflect diffusion in both concentration and band gap gradients over the entire composition range $0 \leq x \leq 1$.[99] In the CdS/Se crystal, diffusion into the bulk is driven by the carrier concentration gradient, which overcomes the opposing potential gradient. The intrinsic decay times of the semiconductors with fixed composition were also required to described the graded results. It was determined that these lifetimes, measured for x = 0, .25, .50, .75, and 1, were dependent upon the microscopic details of the alloy semiconductors. The S versus Se substitution characteristic of the alloy creates disorder induced localized states. Carriers localized at these states encounter fewer nonradiative traps which result in longer observed decay times.

The information obtained from the homogeneous crystals explains the turnover in lifetime trend for the CdSe/S graded semiconductor. The x = .50 composition possesses the largest extent of localization, hence it serves as a "bottleneck". The longer lifetime associated with the x = .50 region becomes competitive with the diffusion from the x = .50 to x = 0 region. As noted previously, the CdS/Se sample includes additional complicating factors, such as self-absorption and reemission effects. However, a bottleneck in the carrier transport and lifetime may explain how different processes could dominate in the separate regions before and after the x = .50 composition. Within a given

homogeneous crystal, the decay functions were not strongly dependent on wavelength. In general, adding a position dependent time constant to Equation 7 would be the first step toward modeling the graded semiconductor results.

Finally, the effect of localization on the diffusion of carriers in the graded CdS_xSe_{1-x} materials is an interesting observation. Transport perpendicular to a composition gradient has also been reported for $Al_xGa_{1-x}As$ superlattices grown by molecular beam epitaxy.[100] In these studies, the transport was observed to be linear over the entire composition range probed (x=.17 to x=.35). That is, no dependence on the lifetime at each composition was observed. As mentioned previously, one may wish to utilize compositional "tuning" to design materials with particular properties. For example, a band gap gradient may be used to transport carriers over a macroscopic distance. Any efforts to tune the CdS_xSe_{1-x} materials will have to account for the trapping at localized states which occur for the strongly mixed compositions.

V. Disorder Induced Localization

A. Background

The experiments on graded CdS_xSe_{1-x} semiconductors, discussed in the previous section, indicate that disorder induced localized states influence the relaxation dynamics of photoexcited e^--h^+ pairs in this system. In this section, the phenomena of disorder induced localization will be discussed in more detail. In these materials, the localized states arise from the compositional disorder of the S versus Se substitution. Since the amount of this disorder can be varied with the mole fraction "x", this system provides a good model for studying the degree of localization as a function of disorder.

The problem of localized states is of long standing and widespread interest. Since Anderson's theory of localization[101] from random potential fluctuations, this subject has been the focus of both theoretical[102-111] and experimental[112-118] interest. The behavior of electrons in complex systems provides a good experimental probe of localization. In the case of alloy materials, electron, hole and electron-hole pair localization have all been observed.[119] Generally, alloy semiconductors provide an excellent probe of localization phenomena, as the conduction normally occurs via extended Bloch states. However, localized states represent nonconducting states in the tail of the band edge.[120,121] Hence, there is a distinct difference between the extended and localized states. This transition in energy is referred to as the "mobility edge". In theory, this transition is distinct, i.e., localized and extended states do not occur at the same energy. In real materials, however, this transition may be gradual. Experimental

studies on localization in semiconductors have often probed the onset of the mobility edge.[121,122] For example, if there is no transfer between localized states, then resonantly excited localized states will retain their initial polarization. Hence, fluorescence polarization experiments yield information on the extent of localization.[123-127]

In CdS_xSe_{1-x} semiconductors, previous work by other researchers has examined the behavior of low temperature excitons in both the binary samples and mixed compositions with time resolved luminescence.[128-133] These studies indicate that the dominant relaxation mechanism at low temperatures is by recombination of localized excitons, where the localized states are due to the alloy disorder. In CdS_xSe_{1-x}, localization occurs via the holes states, the holes are localized and the electrons are Coulombically bound. The dynamics of CdS_xSe_{1-x} excitons at low temperature are dominated by relaxation from these localized states. In this case, a single hop via phonon assisted tunneling determines the transfer rate out of the state, and states at different energies reflect different lifetimes. More specifically, the deeper localized states have fewer states of lower energy to transfer to and hence have longer lifetimes. However, at elevated temperatures, the localized states will affect the carriers in a different manner. Generally, the localization of excitons becomes less important, as the carriers are energetically able to access the regime of extended states. Most likely a series of trapping and release to extended states occurs, as the thermal energy is enough to escape the trapped states.[134] Furthermore, scattering from potential fluctuations affects carrier mobility in these alloy materials. Various estimates have been made for the depth and density of the localized states, ranging from a few to tens of mev.[119,120,130,135] It may

be expected that at high temperature, the behavior of the alloy materials would approach that of the binary semiconductors, CdS and CdSe. However, the previous Section demonstrates a dependence on the compositional disorder for the diffusion in graded CdS_xSe_{1-x}, an effect observed at room temperature. Furthermore, in the preliminary examination of a series of samples with varying degrees of compositional disorder, a large deviation from the binary luminescence exists, even at room temperature. (See results presented in Figure 12.) As mentioned previously, the longer lifetime of $CdS_{.50}Se_{.50}$ is attributed to localization. Localized states possess a higher quantum efficiency and hence, longer lifetime, since localized carriers are less likely to encounter nonradiative decay channels. Figure 13 demonstrates the highly nonexponential form of the luminescence decay in $CdS_{.50}Se_{.50}$. This behavior reflects a dependence on composition which indicates that localized states play a role in the relaxation of carriers even at room temperature. This Section examines the dependence further with additional energy and time resolved luminescence experiments.

The nonexponential functional form for the luminescence decay can be described by a Kohlrausch exponential:

$$I(t) = I(0)\exp(-t/\tau)^{\beta} \qquad (9)$$

This form is a single exponential, with time constant τ, raised to a fractional exponent β. Generally, this form is characterized by a long time "tail" in the decay, hence the term "stretch" exponential is also used. The use of Equation 9 to model data dates back to 1847, when Kohlrausch modeled the nonexponential behavior in viscoelasticity.[136] The Kohlrausch exponential has since been observed as the functional form for a wide variety of relaxation processes in condensed phase.[137-149] The challenge for condensed phase

theories is to provide a microscopic picture that explains the widespread occurrence of the Kohlrausch exponential among different materials (i.e. polymers, glasses, semiconductors) and various types of relaxation (i.e. mechanical, dielectric, photoconductive). The single exponential form arises from noninteracting, independent systems. In this case, the relaxation is then proportional to the remaining perturbation, and a single time constant, t, is sufficient to characterize all dynamic correlations in the system. The underlying physics which result in the Kohlrausch exponential are fundamentally different. In contrast to independent systems, many processes in condensed phase involve strongly interacting systems, or many body interactions. Thus, the widespread appearance of the Kohlrausch exponential in condensed phase corresponds to the frequent occurrence of complex processes which control the dynamics. For example, percolation dynamics result from constrained relaxation, which may be either electronic or structural in origin.[150] In the CdSxSe1-x alloy system, compositional disorder is the source of the complex relaxation.

Furthermore, the mathematical derivation of the stretch exponential decay has been generated from various models, typically proposing either sequential or parallel relaxation pathways.[151-169] Palmer, Stein, Abrahams, and Anderson[151] present a theory based on strongly interacting systems, i.e. "glassy" relaxation, resulting in nonexponential decay dynamics. The authors argue that the basis of the Kohlrausch exponential lies in hierarchically constrained dynamics. These dynamics are a form of sequential relaxation, where the faster degrees of freedom impose constraints on slower ones. A physical example includes atomic motion, whereby atoms must move in a particular way before another degree of freedom can relax. This theory is one of the few

to provide a prediction of the behavior of the parameters as a function of experimental variables, in this case, of temperature. Their model predicts that constrained dynamics will result in nonexponential behavior over a wide range of time scales, $\tau_0 < t < \tau_{max}$, where τ_0 is a time scale relevant to microscopic dynamics (such as 10^{-14}), and τ_{max} is an ergodic time scale. That is, after τ_{max}, the dynamics are single exponential. The theory predicts that as the temperature is lowered below some transition temperature, T_g, then τ_{max} becomes longer than experimentally observable time scales. In the temperature range, $T > T_g$, τ_{max} will vary with temperature according to a Volgel-Fulcher-type behavior:

$$\tau_{max} \sim \exp\left[A/T - T_0\right] \qquad (9)$$

Thus the Palmer, Stein, Abrahams, Anderson model of hierarchical relaxation predicts that as the temperature is lowered, the time scale over which nonexponential dynamics are observed becomes longer. This prediction could be tested experimentally by varying the temperature in the system and carefully modeling the data to extract the behavior of τ.

In a brief review of relaxation in disordered systems, Klafter and Shlesinger[151] demonstrate the underlying mathematical similarity between the Palmer, Stein, Abrahams, Anderson theory and models of both parallel relaxation and defect diffusion. Different physical models are shown to generate the same Kohlrausch relaxation form. The similarity lies in the fact that all three models possess a hierarchy of time scales, as in the constrained dynamics of Palmer, et al. In other models, the hierarchy arises from a dependence on distances (as in Förster energy transfer) or waiting times (in the defect diffusion models). The result is mathematically similar models which do not distinguish

between the underlying physical mechanisms. Hence, it is particularly important for theories to develop connections between the parameters, τ and β, and experimental variables such as temperature or pressure. However, many theories do not contain this information in easily testable form. Much work remains to be done to connect experimentally measurable parameters with the microscopic origin of the relaxation process.

In addition to the model of hierarchically constrained dynamics, a distribution of relaxation times could be responsible for an observed overall nonexponential decay.[170-173] These derivations generally include a weighted distribution, $w(\tau)$, of decay times, such as:

$$I(t) = \int_0^\infty w(\tau)\exp(-t/\tau)d\tau \qquad (10)$$

However, the selection of $w(\tau)$is arbitrary and does not prove a specific relaxation pathway. In this case, a model for the underlying distribution function is required. Qualitatively, the generation of the "stretch" exponential can be understood in terms of a distribution of decay times, as opposed to a single decay channel or perhaps two, in the case of a single or biexponential function. The origin of this distribution in the alloys may arise from the statistical distribution of unit cells generated by the substitution of S versus Se at the lattice sites. This distribution creates local potential fluctuations which induce localized states. These states appear as a tailing of the band edge into the band gap region. Different decay dynamics are associated with relaxation from various localized states, according to, for example, transfer probabilities out of the states, which may depend on the depth and the distance to states of lower energy. If the recombination from these localized states is a major decay channel, then this distribution of relaxation

rates will show up as a Kohlrausch exponential. The parameters in the function, tau and beta, correspond roughly to a characteristic "time constant" of the distribution, and the width of the distribution, respectively. A smaller fractional exponent, beta, reflects a broader distribution of relaxation times. Though this picture presents a qualitative model for the appearance of the stretch exponential form for luminescence decays in alloy semiconductors, a more complete microscopic picture currently does not exist. That is, no model exists to quantitatively connect the amount of disorder induced states with the width of the distribution in Equation 10. Such a connection is required to test the underlying relaxation mechanism in these experiments.

B. Experimental Results and Discussion

This thesis examines the energy and time resolved luminescence of a series of homogeneous CdS_xSe_{1-x} semiconductors. Initial experiments yield evidence for the influence of localized states on the relaxation of photoexcited e^--h^+ pairs. The aim of the following studies is to examine in more detail the composition dependence of the localization effect. As discussed in Section III, a major portion of this research involves the development of luminescence upconversion techniques to probe the dynamics on a picosecond time scale. The purpose of achieving picosecond time resolution is two fold. First, the early time scale components of the luminescence decay functions reflect energy migration which occurs between localized states. Hence, within a given composition material, we expect to determine the wavelength dependence of the decay times, and also the rise time information reflecting the appearance of carriers in the localized states. Furthermore, for the data taken via TCSPC, deconvoluting the instrument function from the measured decay functions was not possible. This effect has severely limited efforts to fit the data and model the extent of localization.

The main experimental details are given in Section III. The differences from the luminescence experiments in Section IV are described here. Picosecond upconversion experiments were completed on three homogeneous CdS_xSe_{1-x} semiconductors, for x = 0, .25, and .50. These experiments were performed with a visible excite energy, typically 10 mw at 580 nm for $CdS_{.25}Se_{.75}$ and CdSe and at 550 nm for $CdS_{.50}Se_{.50}$. At these wavelengths, the optical penetration depth is significantly longer than for the uv excite experiments, .1 μ for uv versus 100 μ for visible excite.[55,56] In these experiments, the

carriers are excited over a greater depth, and the density was typically 10^{16} cm^{-3}. One main result of these different excite wavelengths is to reduce the amount of surface recombination. An additional factor also reduced the surface recombination for these samples. The materials were obtained from Cleveland Crystals as before, but pieces which were cleaved by us were utilized in these experiments. These samples possess a shiny surface by eye, and were not mechanically polished. The reduced surface recombination is observed by the longer decay times for the experiments in this Section, than for the preliminary homogeneous studies in Section IV. Hence, the time constants cannot be compared between the two sets of experiments, as different quality surfaces produce a striking difference in decay times. However, consistent conditions were maintained within the sets of experiments performed in Section IV and here.

The instrument function of the system was measured by autocorrelating Rayleigh scattered light with the gating pulse. This measurement can also be used to determine an absolute t=0. For the fitting, the instrument function was approximated by an analytic function, either a Lorentz or gaussian function. This form was forward convoluted with the fitting function. The data was modeled with an exponential rise and a Kohlrausch decay. Fits to the data were performed by minimizing the sum of the squared errors.

The rise times of all materials studied were extremely fast, less than 3 ps in all cases. Figure 14 shows a typical rise time fit to a <2 ps exponential rise. This result indicates that the intraband cooling is less than 3 ps in these materials. This time is consistent with typical intraband relaxation rates for semiconductors.[174-183] No composition dependence or wavelength dependence was observed in the rise times. In

Figure 14. CdSe Luminescence Rise Time. The early component of the CdSe time resolved luminescence was fit to a <2 ps exponential rise, convoluted with the instrument function for the upconversion spectrometer (in this case, a 1.2 ps Lorentzian pulse). This fast rise time was observed in all of the CdS_xSe_{1-x} materials examined.

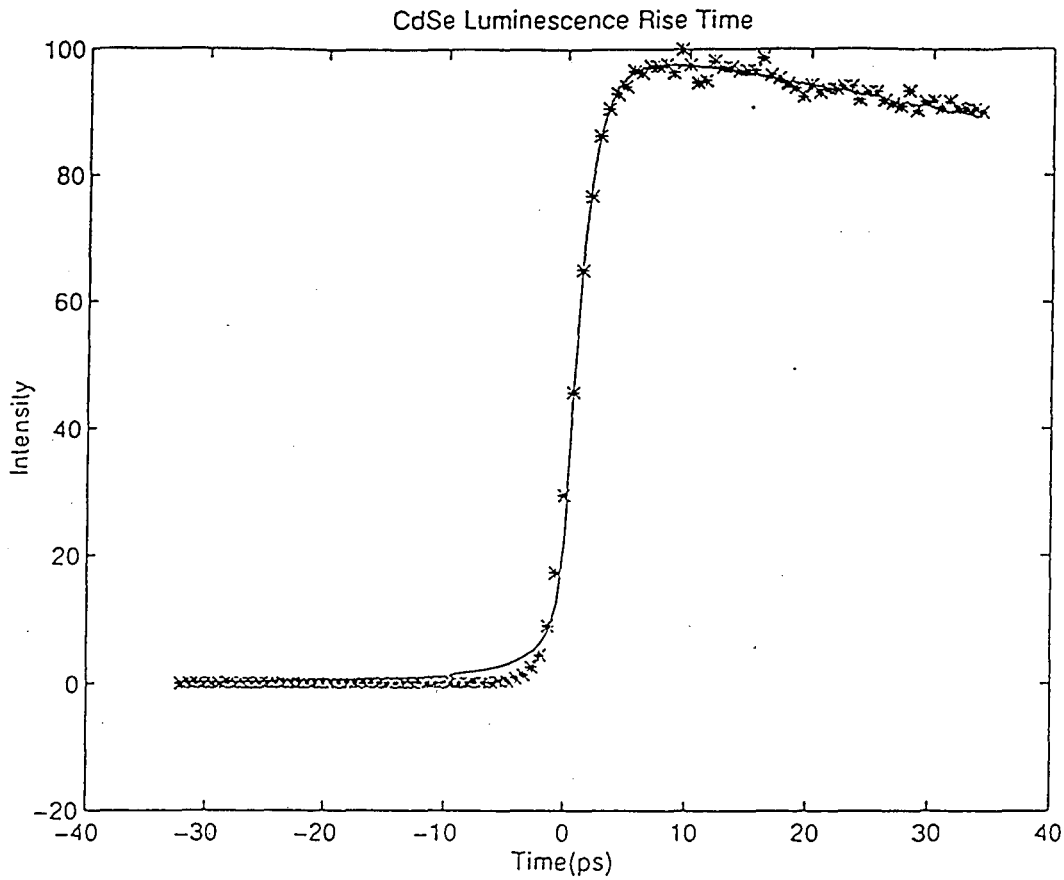
CdSe Luminescence Rise Time
Intensity
Time(ps)
100
80
60
40
20
0
-20
-40
-30
-20
-10
0
10
20
30
40

order to probe the transfer between localized state within the band edge, studies at low temperature need to be performed.

The CdS_xSe_{1-x} luminescence demonstrates a composition dependence on the relaxation times. Figures 15-17 show the data for the three samples studied. Two features are particularly evident. The characteristic time constants for the three samples are from ~ 150-400 ps. Also, the parameter β, which characterizes the distribution, is different for the alloy materials compared to CdSe. The CdSe material is close to single exponential, whereas the $CdS_{.25}Se_{.75}$ and $CdS_{.50}Se_{.50}$ posses a significant amount of nonexponential tailing. It is an interesting result that the time constants are similar in CdSe and $CdS_{.50}Se_{.50}$. Therefore, the longer time luminescence for the alloy material arises from the bowing due to the nonexponential tailing. These results confirm the description of a distribution of localized states present in the mixed composition materials. Furthermore, none of the three samples show significant wavelength dependence. Again, this dependence should be present at low temperature. Transfer among localized state will be slowed as phonon-assisted tunneling is reduced.

Although these results demonstrate the influence of localized states, they do not provide conclusive evidence for a particular relaxation mechanism in these materials. Several steps must be taken to reach that level of quantitative description of the behavior of e^--h^+ pairs in disordered semiconductors. A microscopic model for the influence of disorder on dynamics needs to provide a connection between the amount of localization (i.e. depth and density of states) and parameters in a physical model (such as τ and β in the Kohlrausch exponential). Though much attention has been given to relaxation in disordered systems, the quantitative connection to alloy disorder has not been established.

Further experiments could provide more information to bridge this gap. Investigating the effects of localization in a wider range of compositions may improve theories which estimate the density of localized states in these materials. A complete temperature dependence of the dynamics in the most disordered systems will test models of constrained dynamics, (such as Palmer, et al, discussed above). Such experiments should indicate whether a picture of strongly interacting systems is required to model localized states, or if they can be treated as a distribution of completely independent states. The experiments presented in this thesis demonstrate that localization does influence the relaxation in alloy materials over a large composition range and at room temperature. These results represent a preliminary study of localized states in CdS_xSe_{1-x}. Many future experiments on these materials are warranted.

Figure 15, 16, 17. CdS_xSe_{1-x} time resolved luminescence decays are presented for x = 0,. 25, and .50 materials. The data are fit to a Kohlrausch exponential. The effective time constants for the three materials range from ~ 150 to 400 ps. The longer time tail observed in the $CdS_{.50}Se_{.50}$ luminescence is generated by the smaller fractional exponent in the function. This exponent corresponds to the width of a distribution of lifetimes in the Kohlrausch model.

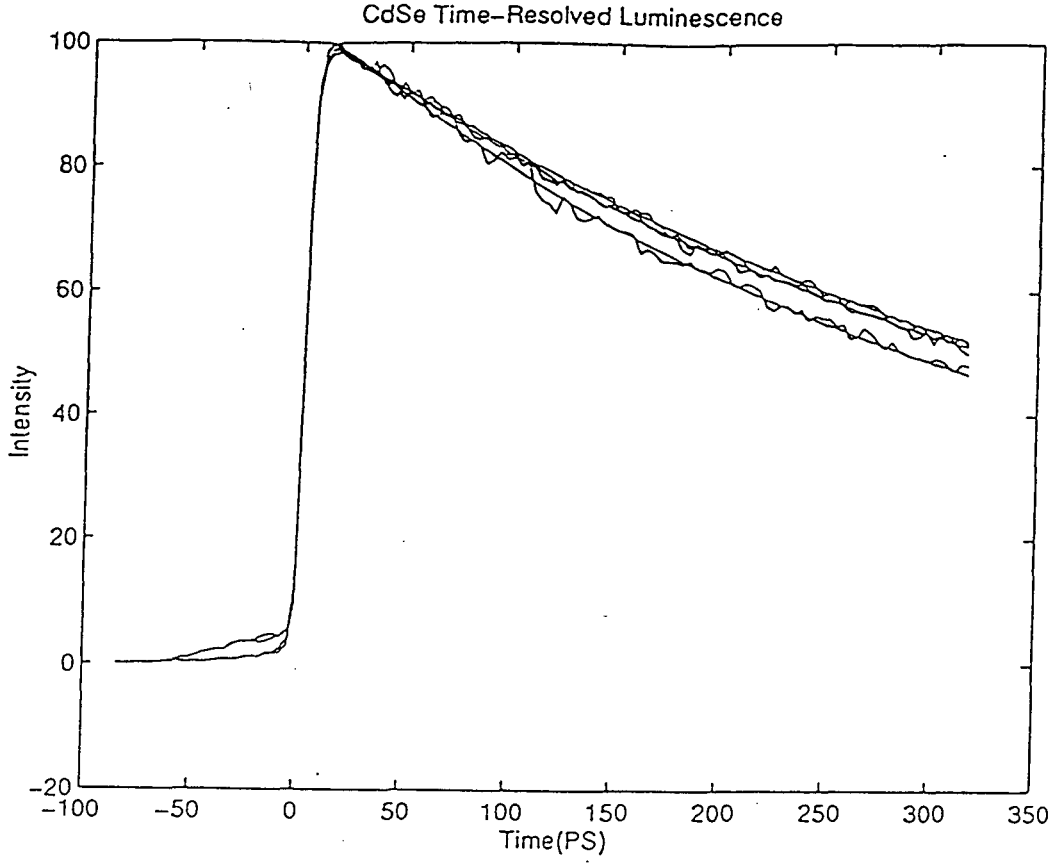

sample	wavelength (nm)	τ (ps)	ß
CdSe	680	387	.88
	690	464	.92
	700	449	.88

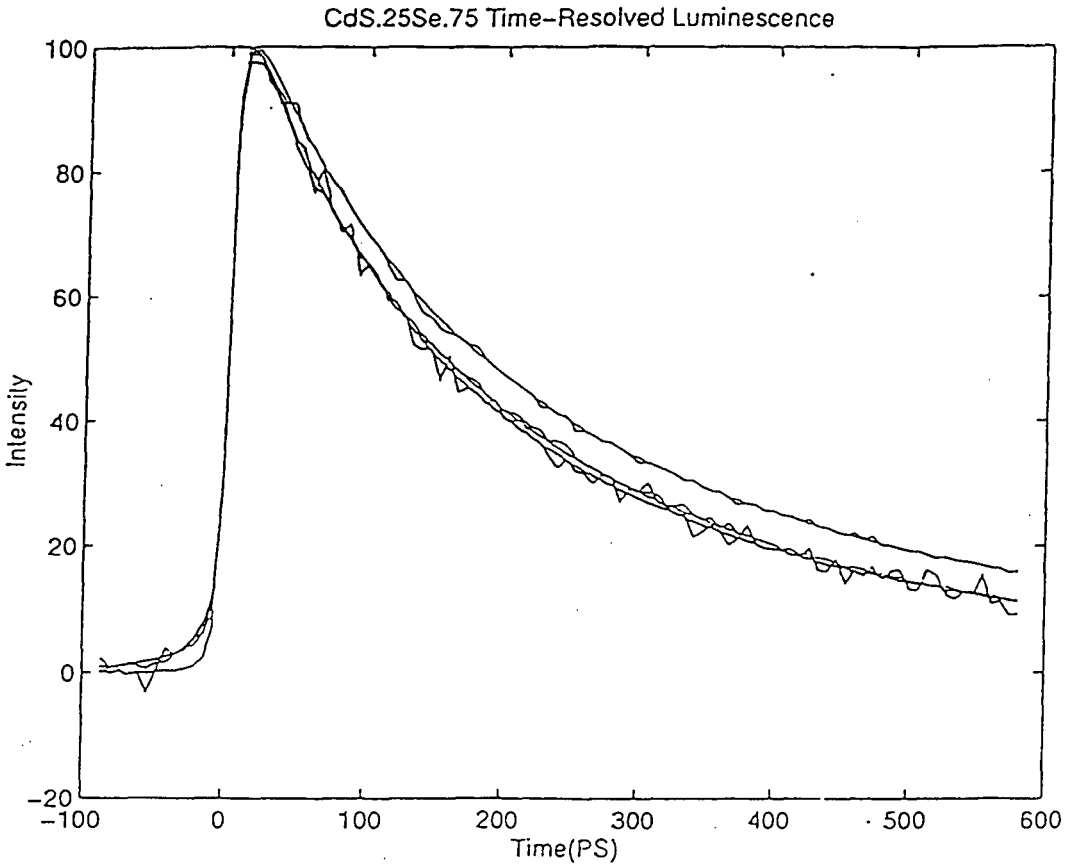

sample	wavelength (nm)	τ (ps)	ß
CdS.25Se.75	640	143	.67
	650	182	.67
	660	160	.70

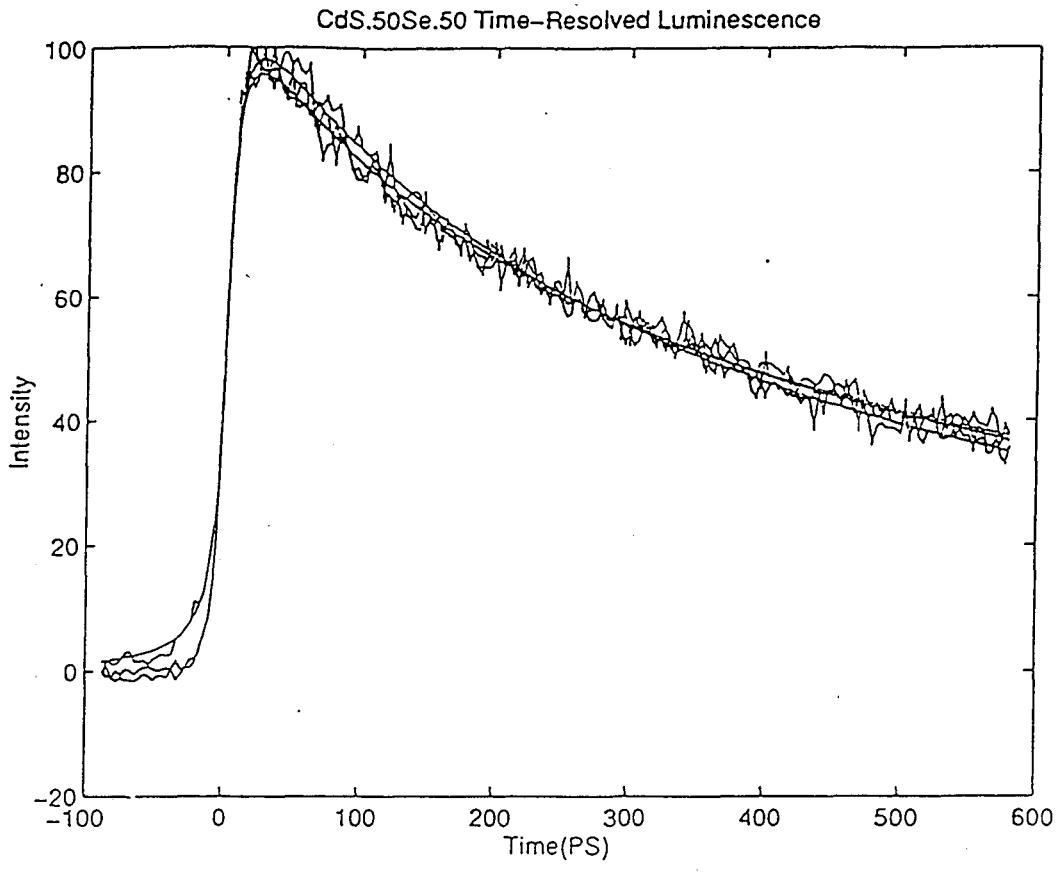

sample	wavelength (nm)	τ (ps)	ß
$CdS_{.50}Se_{.50}$	600	383	.65
	610	399	.58
	620	401	.60

C. Summary

The energy and time resolved luminescence of a series of CdSxSe1-x semiconductors has been measured, with compositions x= 0, .25, and .50. The data were fit to a Kohlrausch, or stretch exponential. The alloy materials show the effect of compositional disorder on carrier relaxation. The decays exhibit a high degree of nonlinearity, which has been attributed to relaxation from a distribution of localized states. All three materials possess time constants of a few hundred picoseconds, (approximately 150 to 400 ps). These measurements were performed under conditions which reduced the amount of surface recombination, and hence the lifetimes were longer here than those presented in Section IV. No wavelength dependence was observed for the rise time or decay functions within a particular composition. Hence, future experiments probing energy transfer among localized states should be performed at low temperature.

The technique of picosecond frequency upconversion was utilized to monitor the carrier relaxation. Upconversion techniques have become increasingly popular for ultrafast luminescence measurements. However, the technique has the limitation of requiring fairly large signal and large laser peak power, since the upconversion process is nonlinear and conversion efficiencies are often small. This work demonstrates that the strong, visible luminescence of the CdSxSe1-x semiconductors is well suited to this measurement technique. Excellent signal-to-noise was achieved and good sensitivity over a wide spectral range was possible.

In conclusion of this Section, these experiments demonstrate the effect of localized states on the relaxation of photoexcited carriers in CdSxSe1-x semiconductors. This effect has been observed both in the transport in graded materials and in the nonexponential luminescence decay of the fixed composition materials. This result addresses one of the principle questions posed in the Introduction. Some optical properties of the CdSxSe1-x system can be described solely as a function of the average composition, such as the shift in band gap as a function "x". Other properties of the system are sensitive to the microscopic, or local environment. In particular, carrier dynamics are affected by potential fluctuations induced from compositional disorder. These potential fluctuations scatter electron-hole pairs, as well as induce localized states which serve as radiative recombination centers.

Theories attempt to map this physical description onto a few parameters, for example, the width of the distribution in the Kohlrausch exponential. However, much work is required to achieve a quantitative and general description of the behavior of localized states. Though disorder induced localization has been observed in many systems, it is interesting that the states are detected in CdSxSe1-x even at room temperature. There are several reasons why the localized states affect the alloy materials to a greater extent than may be expected from simple virtual crystal predictions. The first reason is the difficulty in determining the actual distribution of S versus Se atoms in these materials. This problem is extremely difficult to address, and for a real system, it is unknown whether significant clustering of S or Se atoms occurs. The assumption of a statistical distribution is necessary, as no other detailed picture of the composition is available. Therefore, theoretical predictions of the depth and density of localized states

may not correspond to the samples studied here. Experimental estimates of the mobility edge, i.e. energy at which the switch from localized to extended states occurs, are not sharp, but instead indicate a gradual transition. In theory, localized and extended states cannot exist at the same energy, but experimentally this distinction is not absolute. Hence it is also possible that disorder induced localization influences carriers over a greater energy range than predicted.

VI. REFERENCES

1. Oelgart, G.; Stegmann, R.; John, L. *Phys. Status Solidi A* **1980**, *59*, 27.
2. Pedrotti, F. L.; Reynolds, D. C. *Phys. Rev.* **1962**, *127*, 1584.
3. Handelman, E. T.; Kaiser, W. *J. Appl. Phys.* **1964**, *35*, 3519.
4. Bube, R. H. *J. Appl. Phys.* **1964**, *35*, 586.
5. Park, Y. S.; Reynolds, D. C. *Phys. Rev.* **1963**, *132*, 2450.v
6. Bube, R. H. *Phys. Rev.* **1955**, *98*, 431.
7. Jones, D.; Lettington, A. H. *Solid St. Commun.* **1969**, *7*, 1319.
8. Van Vechten, J. A.; Bergstresser, T. K. *Phys. Rev. B* **1970**, *1*, 3361.
9. Richardson, D. *J. Phys. C: Solid St. Phys.* **1971**, *4*, L289.
10. Nordheim, L. *Physik*, **1931**, *9*, 607.
11. Nordheim, L. *Physik*, **1931**, *9*, 641.
12. Muto, T. *Sci. Papers Inst. Phys. Chem. Research (Tokyo)* **1938**, *34*, 377.
13. Parmenter, R. H. *Phys. Rev.* **1955**, *97*, 587.
14. Hill, R. *J. Phys. C: Solid State Phys.* **1974**, *7*, 521.
15. Streckert, H. H.; Tong, J.; Carpenter, M. K.; Ellis, A. B. *J. Electrochem. Soc.* **1982**, *129*, 772.
16. Streckert, H. H.; Tong, J.; Ellis, A. B. *J. Am. Chem. Soc.* **1982**, *104*, 581.
17. Meyer, G. J.; Lisensky, G. C.; Ellis, A. B. *Proc. Electrochem. Soc.* **1987**, *87-89*, 438.
18. Meyer, G. J.; Lisensky, G. C.; Ellis, A. B. *J. Am. Chem. Soc.* **1988**, *110*, 4914.

19. Murphy, C. J.; Lisensky, G. C.; Leung, L. K.; Kowach, G. R.; Ellis, A. B.; *J. Am. Chem. Soc.* **1990**, *112*, 8344.

20. Evenor, M.; Gottesfeld, S.; Harzion, Z.; Huppert, D.; Feldberg, S. W. *J. Phys. Chem.* **1984**, *88*, 6213.

21. Meissner, D.; Memming, R.; Kastening, B. *J. Phys. Chem.* **1988**, *92*, 3476.

22. Rosenwaks, Y.; Burstein, L.; Shapira, Y.; Huppert, D. *J. Phys. Chem.* **1990**, *94*, 6842.

23. Bessler-Podorowski, P.; Huppert, D.; Rosenwaks, Y.; Shapira, Y. *J. Phys. Chem.* **1991**, *95*, 4370.

24. Handelman, E. T.; Kaiser, W. *J. Appl. Phys.* **1964**, *35*, 3519.

25. Woodbury, H. H.; Hall, R. B. *Phys. Rev.* **1967**, *157*, 641.

26. Taylor, H. F.; Smiley, V. N.; Martin, W. E.; Pawka, S. S. *Phys. Rev. B* **1972**, *5*, 1467.

27. Brillson, L. J.; Conwell, E. M. *J. Appl. Phys.* **1974**, *45*, 5289.

28. Streckert, H. H.; Ellis, A. B. *J. Phys. Chem.* **1982** *86*, 4921.

29. Carpenter, M. K.; Streckert, H. H.; Ellis, A. B. *J. Solid State Chem.* **1982**, *45*, 51.

30. Carpenter, M. K.; Ellis, A. B. *J. Electroanal. Chem.* **1985**, *184*, 289.

31. Sasaki, F.; Mishina, T.; Yasuaki, M.. *Phys. Rev. B*, **1992**, *46*, 6750.

32. Weber, C.; Klingshrin, C.; Chemla, D. S.; Miller, D. A. B.; et al, *Phys. Rev. B* **1988**, *38*, 12748.

33. Wegener, M.; Bar-Joseph, I.; Sucha, G.; Islam, M. N.; et al, *Phys. Rev. B.* **1989**, *39*, 12794.

34. Awschalom, D. D.; et al, *Appl. Phys. Lett.* **1988**, *53*, 2108.

35. Rothberg, L.; Jedju, T. M.; Townsend, P. D.; Etemad, S.; Baker, G. L. **Phys. Rev. Lett.** *1990*, *65*, 100.

36. Stark, J. B.; Knox, W. H.; Chemla, D. S. *Phys. Rev. B.* **1992**, *46*, 7919.

37. Kim, D.-S.; Shah, J.; Cunningham, J. E.; Damen, T. C.; Schmitt-Rink, S.; Schäfer, W. *Phys. Rev. Lett.* **1992**, *68*, 2838.

38. Pantke, K. H.; Norgaard, J.; Erland, J.; Hvam, J. M. *J. Lumin.* **1992**, *53*, 317.

39. Siegner, U.; Weber, D.; Göbel, E. O.; Bennhardt, D.; Heuckeroth, V.; Saleh, R.; Baranovskii, S. D.; Thomas, P.; Schwab, H.; Klingshirn, C.; Hvam, J. M.; Lyssenko, V. G. *Phys. Rev. B* **1992**, *46*, 4564.

40. Dörnfeld, C.; Hvam, J. M. *IEEE J. Quantum Electron.* **1989**, *25*, 904.

41. Weiner, A. M.; De Silvestri, S.; Ippen, E. P. *J. Opt. Soc. Am. B* **1985**, *2*, 654.

42. Schultheis, L.; Sturge, M. D.; Hegarty, *J. Appl. Phys. Lett.* 1985, *47*, 995.

43. Schultheis, L.; Kuhl, J.; Honold, A.; Tu, C. W. *Phys. Rev. Lett.* **1986**, *57*, 1635.

44. Becker, P. C.; Fragnito, H. L.; Brito Cruz, C. H.; Fork, R. L.; Cunningham, J. E.; Henry, J. E.; Shank, C. V. *Phys. Rev. Lett.* **1988**, *61*, 1647.

45. Weber, C.; Becker, U.; Renner, R.; Klingshirn, C. *Z. Phys. B* **1988**, *72*, 379.

46. Hvam, J. M.; Dörnfeld, C.; Schwab, H. In *Nonlinear Optics Materials II*, Grun, J.-B., Ed.; SPIE, **1989**,*1127*, 59.

47. Hvam, J. M.; Lyssenko, V. G.; Schwab, H. *J. Crystal Growth* **1992**, *117*, 773.

48. Schwab, H.; Lyssenko, V. G.; Hvam, J. M. *Phys. Rev. B* **1991**, *44*, 3999.

49. Noll, G.; Seigner, U.; Shevel, S. G.; Göbel, E. O. *Phys. Rev. Lett.* **1990**, *64*, 792.

50. O'Connor, D. V.; Phillips, D. *Time-correlated Single Photon Counting*; Academic Press: London, **1984**.

51. Badea, M. G.; Brand, L. *Meth. Enzymol.* **1979**, *61*, 378.

52. Birks, J. B.; Munro, J. H. *Prog. Reac. Kinet.* **1967**, *4*, 239.

53. Isenberg, J. In *Biochemical Fluorescence Concepts*, Chem, R. F.; Edelhoch, H., Eds.; Marcel-Dekker: New York, **1975**, *Vol. 1*, 43.

54. Knight, A. E. W.; Selinger, B. K. *Aust. J. Chem*, **1973**, *26*, 1.

55. Poultney, S. K. *Adv. Elect. Phys.* **1972**, *31*, 39.

56. Ware, W. R. In *Creation and Detection of the Excited State*, Lamola, A., Ed.; Marcel-Dekker: New York, **1971**, *Vol. 1A*, 213.

57. Yguerabide, J. *Meth. Enzymol.* **1972**, *26*, 498.

58. Ghiggino, K. P.; Roberts, A. J.; Phillips, D. *J. Phys. E.* **1980**, *13*, 446.

59. Schwartz, B. J; Ph.D. Thesis, UC Berkeley, **1992**.

60. Shen, Y. R. *ThePrinciples of Nonlinear Optics*; Wiley: New York, **1984**.

61. Zernike, F.; Midwinter, J. E. *Applied Nonlinear Optics*; Wiley: New York, **1973**.

62. Shah, J. *IEEE J. Quantum Electron.* **1988**, *24*, 276.

63. Mahr, H.; Hirsch, M. D. *Opt. Commun.* **1975**, *13*, 96.

64. Daly, T.; Mahr, H. *Solid State Commun.* **1978**, *25*, 323.

65. Hirsch, M. D.; Mahr, H. *Chem. Phys. Lett.* **1979**, *60*, 299.

66. Mahr, H.; Daly, T.; Frigo, N. J. In *Picosecond Phenomena*, Shank, C. V.; Ippen, E. P.; Shapiro, S. L., Eds.; Springer-Verlag: Berlin, **1978**, 230.

67. Hirsch, M.; Marcus, M. A.; Lewis, A.; Mahr, H. *Biophys. J.* **1976**, *15*, 1399.

68. Hallidy, L. A.; Topp, M. R. *Chem. Phys. Lett.* **1977**, *46*, 8.

69. Hallidy, L. A.; Topp, M. R. *Chem. Phys. Lett.* **1977**, *48*, 40.

70. Hallidy, L. A.; Topp, M. R. *J. Phys. Chem.* **1978**, *82*, 2415.

71. Hallidy, L.; Horn-Bond Lin; Topp, M. In *Picosecond Phenomena*, Shank, C. V.; Ippen, E. P.; Shapiro, S. L., Eds.; Springer-Verlag: Berlin, **1978**, 230.

72. Simon, J. D. *Rev. Sci. Instrum.* **1989**, *60*, 3597.

73. Kash, K.; Shah, J. *Appl. Phys. Lett.* **1984**, *45*, 401.

74. Shah, J.; Damen, T. C.; Deveaud, B.; Block, D. *Appl. Phys. Lett.* **1987**, *50*, 1307.

75. Elsaesser, T.; Shah, J.; Rota, L; Lugli, P. *Phs. Rev. Lett.* **1991**, *66*, 1757.

76. Damen, T. C.; Shah, J. *Appl. Phys. Lett.* **1988**, *52*, 1291.

77. Kahlow, M. A.; Jarzeba, W.; DuBruil, T. P.; Barbara, P. F. *Rev. Sci. Instrum.* **1988**, *59*, 1098.

78. Barbara, P. F.; Kahlow, M. A. *AIP Conf. Proceed.* **1988**, *172*, 724.

79. Elsaesser, T.; Shah, J.; Rota, L.; Lugli, P. *Semicond. Sci. Technol.* **1992**, *7*, B144.

80. Shah, J.; Damen, T. C.; Tsang, W. T.; Gossard, A. C.; Lugli, P. *Phys. Rev. Lett.* **1987**, *59*, 2222.

81. Freeman, M. R.; Awschalom, D. D.; Hong, J. M.; Chang, L. L. *Phys. Rev. Lett.* **1990**, *64*, 2430.

82. Freeman, M. R.; Awschalom, D. D. *J. Appl. Phys.* **1990**, *67*, 5102.

83 Freeman, M. R.; Awschalom, D. D.; Hong, J. M.; Chang, L. L. *Surface Sci.* **1990**, *228*, 233.

84. Kahlow, M. A.; Kang, T. J.; Barbara, P. F. *J. Chem. Phys.* **1988**, *88*, 2372.

85. Kahlow, M. A.; Jarzeba, W.; Kang, T. J.; Barbara, P. F. *J. Chem. Phys.* **1989**, *90*, 151.

86. Ruggiero, A. J.; Todd, D. C.; Fleming, G. R. *J. Am. Chem. Soc.* **1990**, *112*, 1003.

87. Du, M.; Xie, X.; Jia, Y.; Mets, L.; et al, *Chem. Phys. Lett.* **1993**, *201*, 535.

88. Rosenthal, S. J.; Xie, X.; Du, M..; Fleming, G. R. *J. Chem. Phys.* **1991**, *95*, 4715.

89. Todd, D. C.; Jean, J. M.; Rosenthal, S. J.; Ruggiero, A. J.; et al, *J. Chem. Phys.* **1990**, *93*, 8658.

90. Castner, E. W., Jr.; Bagchi, B.; Maroncelli, M.; Webb, S. P.; et al, *Berichte der Bunsengesellschaft fur Physikalische Chemie*, **1988**, *92*, 363.

91. Castner, E. W., Jr.; Maroncelli, M.; Fleming, G. R. *J. Chem. Phys.* **1987**, *86*, 1090.

92. Freeman, M. R.; Awschalom, D. D.; Hong, J. M. *Appl. Phys. Lett.* **1990**, *57*, 704.

93. Dutton, D. *Phys. Rev.* **1958**, *112*, 785.

94. Parson, R. B.; Wardzynski, W.; Yoffe, A. D. *Proc. R. Soc. London A* **1961**, *262*, 120.

95. Van Ruyven, L. J.; Williams, F. E. *Am. J. Phys.* **1967**, *35*, 705.

96. Dumke, W. P. *Phys. Rev.* 1963, *132*, 1998.

97. Madelung, O.; Schultz, M.; Weiss, H.; Eds. In *Landolt-Bornstein Numerical Data and Functional Relationships in Science and Technology*; Hellwege, K.-H., Editor-in-Chief; Springer-Verlag: Berlin, **1982**, *New Series, Vol. 17b*, pp 190, 217.

98. Gourdon, C.; Lavallard, P.; Permogorov, S.; Reznitsky, A. *J. Lumin.* **1988** *39*, 269.

99. Hane, J. K.; Prisant, M. G.; Harris, C. B.; Meyer, G. J.; Leung, L. K.; Ellis, A. B. *J. Phys. Chem.* **1989**, *93*, 7975.

100. Deveaud, B.; Shah, J.; Damen, T. C.; Lambert, B.; Regreny, A. *Phys. Rev. Lett.* **1987**, *58*, 2582.

101. Anderson, P. W. *Phys. Rev.* **1958**, *109*, 1492.

102. Abrahams, E.; Anderson, P. W.; Licciardello, D. C.; Ramakrishnan, T. V. *Phys. Rev. Lett.* **1979**, *42*, 673.

103. Thouless, D. J. *J. Phys. C: Solid St. Phys.* **1970**, *3*, 1559.

104. Thouless, D. J. *J. Phys. C: Solid St. Phys.* **1972**, *5*, 77.

105. Ziman, J. M. *J. Phys. C: Proc. Phys. Soc.* **1968**, *1*, 1532.

106. Ziman, J. M. *J. Phys. C: Solid St. Phys.* **1969**, *2*, 1230.

107. Thouless, D. J. *Phys. Rev.* **1974**, *13*, 93.

108. Thouless, D. J. *Phys. Rev. Lett.* **1977**, *39*, 1167.

109. Thouless, D. J. In *Ill Condensed Matter*,Toulouse, G.; Balian, R., Eds.; North Holland: Amsterdam, 1979, 1.

110. Mott, N. F.; Davis, E. A. *Electronic Processes in Non-Crystalline Material*, 2nd ed., Clarendon: Oxford, **1979**.

111. Lee, P. A.; Ramakrishnan, T. V. *Rev. Mod. Phys.* **1985**, *57*, 287.

112. Scher, H.; Montroll, E. W. *Phys. Rev. B* **1975**, *12*, 2455.

113. Bos, F. C.; Burland, D. M. *Phys. Rev. Lett.* **1987**, *58*, 152.

114. Jiang, H. X.; Lin, J. Y. *Phys. Rev. Lett.* **1990**, *64*, 2547.

115. Jiang, H. X.; Lin, J. Y. *Phys. Rev. B* **1989**, *40*, 10025.

116. Lin, J. Y.; Jiang, H. X. *Phys. Rev. B* **1990**, *41*, 5178.

117. Jiang, H. X.; Zu, L. Q.; Lin, J. Y. *Phys. Rev. B* **1990**, *42*, 7284.

118. Lingle, R. L.; Padowitz, D. F.; Jordan, R. E.; McNeill, J. D.; Harris, C. B. *Phys. Rev. Lett.* **1994**, *72*, 2243.

119. Ouadjaout, D.; Marfaing, Y.; *Phys. Rev. B* **1990**, *41*, 12096.

120. Baranovskii, S. D.; Efros, A. L. *Sov. Phys. Semicond.* **1978**, *12*, 1328.

121. Cohen, E.; Sturge, M. D. *Phys. Rev. B* **1982**, *25*, 3828.

122. Kash, J. A.; Ron, A.; Cohen, E.; *Phys. Rev. B* **1983**, *28*, 6147.

123. Permogorov, S.; Reznitsky, A.; Verbin, S.; Lysenko, V. *Solid State Comm.* 1983, *47*, 5.

124. Permogorov, S.; Rezmitsky, A.; Travnikov, V.; Verbin, S.; Muller, G. O.; Nikiforova, M. *J. Lumin.* **1981**, *24/25*, 413.

125. Permogorov, S. A.; Reznitskii, A. N.; Verbin, S. Y.; Lysenko, V. G. *JEPT Lett.* **1983**, *37*, 462.

126. Verbin, S. Y.; Permogorov, S. A.; Reznitskii, A. N. *Soviet Phys. Solid State* **1983**, *25*, 195.

127. Schwab, H.; Lyssenko, V. G.; Reznitsky, A. N.; Klingshirn, C. *J. Lumin.* **1991**, *48/49*, 661.

128. Shevel, S.; Fischer, R.; Gobel, E. O.; Noll, G.; Thomas, P.; Klingshirn, C. *J. Lumin.* **1987**, *37*, 45.

129. Gourdon, C.; Lavallard, P.; Permogorov, S.; Reznitsky, A.; Aaviksoo, Y.; Lippmaa, Y. *J. Lumin.* **1987**, *39*, 111.

130. Gourdon, C.; Lavallard, P.; Permogorov, S.; Reznitsky, A. *J. Lumin.* **1988**, *39*, 269.

131. Swoboda, H.-E.; Majumder, F. A.; Klingshirn, C.; Shevel, S.; Fischer, R.; Gobel, E. O.; Noll, G.; Thomas, P.; Permogorov, S.; Reznitsky, A. *J. Lumin.* **1987**, *38*, 79.

132. Urban, M.; Schwab, H.; Klingshirn, C. *Phys. Stat. Sol.* **1991**, *166*, 423.

133. Gourdon, C.; Lavallard, P. *Phys. Stat. Sol.* **1989**, *153*, 641.

134. Scher, H.; Montroll, E. W.; *Phys. Rev. B* **1975**, *12*, 2455.

135. Majumder, F. A.; Shevel, S.; Lyssenko, V. G.; Swoboda, H. E.; Klingshirn, C. *Z. Phys. B- Cond. Matter* **1987**, *66*, 409.

136. Kohlrausch, R. *Ann. Phys. (Leipzig)* **1847**, *12*, 393.

137. Shlesinger, M. F. *Ann. Rev. Phys. Chem.* **1988**, *39*, 269.

138. Jonscher, A. K. In *Structure and Bonding in Noncrystalline Solids*; Walrafen, G. E.; Revesz, A. G., Eds. Plenum: New York, **1986**, 101.

139. Montroll, E. W.; Bendler, J. T. *J. Stat. Phys.* **1984**, *34*, 129.

140. Williams, G.; Watts, D. C. *Trans. Faraday Soc.* **1970**, *66*, 80.

141. Chamberlin, R. V.; Mozurkewich, G.; Orbach, R. *Phys. Rev. Lett.* **1984**, *52*, 867.

142. Even, U.; Rademann, K.; Jortner, J.; Manor, N.; Reisfeld, R. *Phys. Rev. Lett.* **1984**, *52*, 2164.

143. Blumen, A.; Klafter, J.; Zumofen, G. In *Optical Spectroscopy of Glasses*, Zschokke, I., Ed.; Reidel: Dordrecht, **1986**, 199.

144. Austin, R. H.; Beeson, K. W.; Eisenstein, L.; Frauenfelder, H.; Gunsalus, I. C. *Biochem.* **1975**, *14*, 5355.

145. Ansari, A.; Berendzen, Y.; Bowne, S. F.; Frauenfelder, H.; Iben, I. E. T.; Sauke, T. B.; Shyamsunder, E.; Young, R. D. *Proc. Nat. Acad. Sci.* **1985**, *82*, 5000.

146. Hopfield, J.; Tenk, D. W. *Science* **1985**, *233*, 625.

147. Kirkpatrick, S.; Gelatt, C. D., Jr.; Vecchi, M. P. *Science* **1983**, *220*, 671.

148. Mezei, F.; Murani, A. P. *Magn. Mater.* **1979**, *14*, 211.

149. Pfister, G.; Scher, H. *Adv. Phys.* **1978**, *27*, 747.

150. Knapp, E. W. *Phys. Rev. Lett.* **1988**, *60*, 2386.

151. Palmer, R. G.; Stein, D. L.; Abrahams, E.; Anderson, P. W. *Phys. Rev. Lett.* **1984**, *53*, 958.

152. Klafter, J.; Shlesinger, M. F. *Proc. Natl. Acad. Sci. USA* **1986**, *83*, 848.

153. Rajagopal, A. K.; Ngai, K. L.; Teitler, S. *Physica* **1986**, 359.

154. Lindsey, C. P.; Patterson, G. D. J. Chem. Phys. **1980**, *73*, 3348.

155. Shore, J. E.; Zwanzig, R. *J. Chem. Phys.* **1975**, *63*, 5445.

156. Cohen, M. H.; Grest, G. S. In *Structure and Mobility in Molecular and Atomic Glasses*, O'Reilly, J. M.; Goldstein, M., Eds.; Academic: New York, **1981**, 199.

157. Ngai, K. L.; White, C. T. *Phys. Rev. B* **1979**, *20*, 2475.

158. Skinner, J. L. *J. Chem. Phys.* **1983**, *79*, 1955.

159. Shlesinger, M. F.; Montroll, E. W. *Proc. Natl. Acad. Sci. USA* **1984**, *81*, 1280.

160. Klafter, J.; Blumen, A. *Chem. Phys. Lett.* **1985**, *119*, 377.

161. Förster, T. Z. *Naturforsch. Teil A* **1949**, *4*, 321.

162. Blumen, A. *Neuvo Cimento Soc. Ital. Fis. B* **1981**, *63*, 50.

163. Klafter, J.; Blumen, A. *J. Chem. Phys.* **1984**, *80*, 875.

164. Huberman, B. A.; Kerszberg, M. *J. Phys. A* **1985**, *18*, L331.

165. Glarum, S. H. *J. Chem. Phys.* **1960**, *33*, 1371.

166. Jonscher, A. K. *Nature*, **1977**, *267*, 673.

167. Ngai, K. L. *Comments Solid State Phys.* **1979**, *9*, 127.

168. Ngai, K. L. *Comments Solid State Phys.* **1980**, *9*, 141.

169. Cohen, M. H.; Grest, G. S. *Phys. Rev. B* **1981**, *24*, 4091.

170. Davidson, D. W.; Cole, R. H. *J. Chem. Phys.* **1951**, *19*, 1417.

171. Moynihan, C. T.; Gupta, P. K. *J. Non-Crystalline Solids* **1978**, *29*,143.

172. Moynihan, C. T.; Boesch, L. P.; LaBerge, N. L. *Phys. Chem. Glasses* **1973**, *14*, 122.

173. Montrose, C. J.; Litovitz, T. A. J. *Acoust. Soc. Am.* **1970**, *47*, 1250.

174. Shah, J.; Leite, R. C. C. *Phys. Rev. Lett.* **1979**, *22*, 1304.

175. von der Linde, C.; Lambrich, R. *Phys. Rev. Lett.* **1979**, *42*, 1090.

176. Chebira, A.; Chesnoy, J.; Gale, G. M. *Phys. Rev. B* **1992**, *46*, 4559.

177. Shank, C. V.; Fork, R. L.; Yen, R.; Shah, J.; et al, *Solid State Commun.* 1983, *47*, 981.

178. Shah, J. Leheny, R. F.; Nahory, R. E.; Pollack, M. A. *Appl. Phys. Lett.* **1980**, *37*, 475.

179. Shah, J. *Solid State Electron.* **1989**, *32*, 1051.

180. Kash, K.; Shah, J. *J. Lumin.* **1985**, *30*, 333.

181. Kash, K.; Shah, J.; Block, D.; Gossard, A. C.; et al, *Physica B & C*, **1985**, *134 B/C*, 189.

182. Vengurlekar, A. S.; Prabhu, S. S.; Roy, S. K.; Shah, J. *Phys. Rev. B* **1994**, *50*, 15461.

183. Sucha, G.; Bolton, A. S. R.; Chemla, D. S.; Sivco, D. I. *Appl. Phys. Lett.* **1994**, *65*, 1486.

LAWRENCE BERKELEY LABORATORY
UNIVERSITY OF CALIFORNIA
TECHNICAL INFORMATION DEPARTMENT
BERKELEY, CALIFORNIA 94720